Post-depositional modification on seasonal and interannual timescales resets the deuterium excess signals in summer snow layers in Greenland

M. S. Town[1], H. C. Steen-Larsen[1], S. Wahl[1,2], A.-K. Faber[1], M. Behrens[3], M. Hörhold[3], T. R. Jones[4], A. Sveinbjornsdottir[5], A. M. Zuhr[6]

[1]Geophysical Institute and Bjerknes Centre for Climate Research, University of Bergen, Bergen, Norge
[2]École Polytechnique Fédérale de Lausanne, Lausanne, Suisse
[3]Alfred-Wegener-Institut Helmholtz-Zentrum für Polar- und Meeresforschung, Research Unit Bremerhaven, Bremerhaven, Germany
[4]Institute of Arctic and Alpine Research, University of Colorado, Boulder, USA
[5]Institute of Earth Sciences, Reykjavík, Ísland
[6]Alfred-Wegener-Institut Helmholtz-Zentrum für Polar- und Meeresforschung, Research Unit Postdam, Postdam, Germany

Key Points:

- Deuterium-excess (d) decreases up to 5 $^{o}/_{oo}$ in near-surface snow during some summers at EastGRIP, likely due to net sublimation.
- After one-to-two years in the snowpack, the peak d shifts from Autumn snow layers towards Summer snow layers.
- Isotope-gradient diffusion explains some but not all of the d seasonality changes in the near-surface snow.

Corresponding author: Michael S. Town, michael.town@uib.no

Corresponding author: Hans Christian Steen-Larsen, hans.christian.steen-larsen@uib.no

Abstract

We document the isotopic evolution of near-surface snow at the EastGRIP ice core site in the Northeast Greenland National Park using a time-resolved array of 1-m deep isotope ($\delta^{18}O$, δD) profiles. The snow profiles were taken from May-August during the 2017-2019 summer seasons. An age-depth model was developed and applied to each profile mitigating the impacts of stratigraphic noise on isotope signals. There is a decrease in seasonal isotope-temperature sensitivity over 1.5 years of aging ($^{\Delta\delta^{18}O}/_{\Delta T}/\Delta$t $= 0.096\pm0.04\,^{o}/_{oo}\cdot\,^{o}C^{-1}\cdot\mathrm{yr}^{-1}$). Isotopic changes *can* occur during summer seasons (increase in $\delta^{18}O$, decrease in d-excess, d). After one year of aging the same summer layers always experience a 3-5 $^{o}/_{oo}$ increase in d. Thus, d does not just carry information about source region conditions and transport history, but also integrates local conditions into summer snow layers as the snow ages. No significant change is observed in $\delta^{18}O$ on interannual time scales. Isotopic-gradient-driven diffusion occurs throughout the year. It is most impactful in the summer seasons but does not explain all changes we observe. Other mechanisms of post-depositional processes are inferred to be net sublimation from surface and near-surface snow in summer seasons, and vapor-pressure-gradient driven exchange within the near-surface snow during shoulder seasons. Our results are dependent on the site characteristics (e.g. wind, temperature, accumulation rate), but indicate that more process-based research is necessary to understand water-isotope-to-climate proxies. Recommendatiosn for monitoring and physical modeling are given, with special attention to the d-excess parameter.

Plain Language Summary

The relative abundance of heavy water isotopes have been used effectively to understand the past climates of polar regions and beyond. Oxygen-18 in snow is thought to be a proxy for the local cloud or surface temperature. Deuterium excess, a derivative of heavy water isotopes, is considered an integrated history of water from source to deposition. We present data from a three-year study of near-surface snow at a polar ice core site in Northeast Greenland. Comparing annually successive samples of the same snow layers, we track changes in the snow after it is deposited. We date each snow layer to compare and average related layers. Net sublimation during summer sometimes enriches the snow's oxygen-18, making it seem warmer than it actually was. Summertime sublimation also causes the deuterium excess to indicate that the snow came from closer

or more humid places. After a year or more of aging, summer snow layers nearly regain their original deuterium excess signal. Open questions remain, and we recommend future field work and modeling to investigate these questions. Highly-trained and observationally-verified models can then be used to refine interpretation of polar ice cores.

1 Introduction

The relative concentration of stable water isotopes from polar snow and ice have proven useful in telling warm from cold in reconstructions of Earth's past climate (e.g., Lorius et al., 1990; Jouzel et al., 1997; Johnsen et al., 2001; Jouzel et al., 2003; Kavanaugh & Cuffey, 2003; Steig et al., 2013). In the past, climate reconstructions were dependent on understanding the sensitivity of changes in water isotopes to changes in mean annual temperature in the polar regions, i.e., the water-isotope-temperature sensitivity. Small changes in this sensitivity had significant influence on inferences about past climates based on polar ice cores (e.g., P. Grootes et al., 1993; Charles et al., 1994; Petit et al., 1999; Jouzel et al., 2003). Recent climate reconstruction efforts are not as dependent on temperatures inferred from water isotopes in polar snow, rather using an array of globally distributed proxies (e.g., Rohling et al., 2012; Dahl-Jensen et al., 2013; Buizert et al., 2021). However, simulation of past polar ice sheet mass balance and climate still require accurate knowledge of ice sheet temperatures often derived from empirical isotope-temperature sensitivities (e.g., Cuffey et al., 2016; Jones et al., 2023). Past circulation and weather patterns are also possible to derive from combinations of isotope and other chemistry measurements from polar snow and ice (e.g., Mayewski et al., 1994; Steffensen et al., 2008; Guillevic et al., 2013; Jones et al., 2018). Such understanding is important not only to make claims about past climate, but to improve models for prediction of weather and future climate (e.g., Blossey et al., 2010; Werner et al., 2011; Dee et al., 2015; Dütsch et al., 2019).

Despite the importance of accurate understanding the connection of isotope signals in polar snow and ice to climate, there is a lack of continuous understanding of how climate is imprinted in the isotopic composition of polar snow, from moisture source to eventual ice core extraction and analysis. Specifically, there is much to learn about what happens to the isotopic signal in the top meter of snow when it is still under the influence of local meteorology. This study provides observations that document relevant meteorology-

induced isotopic changes in surface and near-surface snow that provokes a revised interpretation of the water isotope climate proxy.

1.1 Nomenclature

Here, we will use established nomenclature to discuss the concentration of heavy water isotopes in vapor, precipitation, or snow (Craig & Gordon, 1965; Dansgaard, 1964). Equation 1 shows the relative concentration of heavy water $H_2^{18}O$ to the more predominant lighter isotope (e.g., $H_2^{16}O$) in reference to the same isotopic ratio from a standard water source, the Vienna Standard Mean Ocean Water (VSMOW, Craig, 1961; Gonfiantini, 1978).

$$\delta^{18}O = \left(\frac{\frac{H_2^{18}O}{H_2^{16}O}_{sample}}{\frac{H_2^{18}O}{H_2^{16}O}_{VSMOW}} - 1\right) * 1000 \tag{1}$$

The water-isotope-temperature sensitivity is then defined as equation 2 for $\delta^{18}O$.

$$\gamma = \frac{\Delta\delta^{18}O}{\Delta T} \tag{2}$$

This relationship can be defined from either spatially-distributed data sets (i.e. γ_s), or temporally-derived data sets (i.e. γ_t). A linear pattern has been observed between spatially-distributed measurements of mean annual temperature and mean annual water isotope content of precipitation and surface snow, which we call γ_s (e.g. Dansgaard, 1964). Here ΔT usually represents the change in mean annual temperature associated with a change in $\delta^{18}O$ (i.e. $Delta\delta^{18}O$). It has iteratively been realized that γ_s represents integrated temperature and distillation effects, as well as source region characteristics (Merlivat & Jouzel, 1979; Jouzel & Merlivat, 1984; Ciais & Jouzel, 1994). The water-isotope-temperature sensitivity can also be defined using observation- or model-based temporal variations of $\delta^{18}O$ and temperature for a location (e.g., γ_t, Cuffey et al., 1995, 2016; Werner et al., 2018). The temporal water-isotope-sensitivity, γ_t, is not necessarily the same as a $\gamma_s$for a similar region or climate.

Under equilibrium conditions, there is a linear pattern between $\delta^{18}O$ and the relative concentration of deuterium-laden water, δD(Dansgaard, 1964). The intercept of this relationship is commonly referred to as 'deuterium excess' (d-excess or d, equation

3; e.g., Merlivat & Jouzel, 1979; Jouzel & Merlivat, 1984). It is used as an integrated characterization of an air mass's water vapor and precipitation history. The mean value for equation 3 for global precipitation is 10 $^{o}/_{oo}$ (Dansgaard, 1964). In polar snow, d is expected to peak in Autumn precipitation and snow layers, and be a minimum in Spring precipitation and snow layers (Johnsen & White, 1989), influenced by sea ice extent, proximity to moisture source, and moisture source sea surface temperature. However, a summertime peak in d has recently been observed in precipitation at Summit, Greenland (Kopec et al., 2022).

$$d = \delta D - 8 * \delta^{18}O \tag{3}$$

Statistically, we are mainly concerned with how mean values compare even as distributions of these isotopic values and their derivatives (i.e., $\delta^{18}O$ and d) may overlap. As such, most of our error values and uncertainty ranges are represented as two times the standard error around the means ($2\sigma_{\bar{x}}$, $p < 0.05$). Where the overlap of distributions are important we report two times the standard deviation around the mean (i.e., 2σ).

When we discuss the influence of the near-surface atmosphere on the surface and near-surface snow, we will use the following definitions unless otherwise stated. The near-surface atmosphere is the atmospheric surface layer (e.g., Mahrt, 2014) where mechanical shear generates more turbulence than buoyancy generates or consumes. In the stable boundary layers on polar ice sheets it can range from 10 m to 10s of meters thick depending on the inversion strength and wind speed (e.g., Hudson & Brandt, 2005; King & Turner, 2009). Operational definitions for surface snow and near-surface snow are 0-1 cm and 0-100 cm, respectively.

1.2 From source to sink

Isotope-enabled models (IEMs) of regional-to-global extent are now employed to probe complex relationships between water isotopes, including evaporative processes at the source, mixing and cloud physics processes along the way, and final precipitation physics (e.g., Blossey et al., 2010; Dee et al., 2015; Dütsch et al., 2019; Hu et al., 2022; Werner et al., 2011). Some focus is still on water-isotope-temperature relationships like γ_t (e.g., Werner et al., 2018). Yet, it is recognized that a more comprehensive, process-based ap-

proach to isotope-climate relationships is necessary. The hydrologic cycle is then a primary focus of IEMs and their low-complexity predecessors (e.g., Merlivat & Jouzel, 1979; Jouzel & Merlivat, 1984; Johnsen & White, 1989; Ciais & Jouzel, 1994; Blossey et al., 2010; Werner et al., 2011). IEMs of a range of complexity have opened up nuanced, integrated interpretation of isotope concentration derivatives like d, advancing modeled hydrologic processes and interpretation of ice cores (e.g. Merlivat & Jouzel, 1979; Jouzel & Merlivat, 1984; Blossey et al., 2010; Dütsch et al., 2019; Hu et al., 2022).

1.3 From sink to extraction

After deposition at a polar site, the isotopic content of snow is not 'locked in place' (e.g., Steen-Larsen et al., 2014), but continues to evolve in response to its surrounding environment. Deeper in the firn and ice column (>2 m) and over longer time periods, diffusion along isotopic gradients become a dominant smoothing process (Johnsen, 1977; Johnsen et al., 2000; Gkinis et al., 2014; Jones et al., 2017). Proper inversion of this process is necessary for accurate reconstruction of timing and magnitude of isotopic signals (e.g., Johnsen et al., 2000; Vinther et al., 2010; Jones et al., 2018, 2023), although we show here that additional isotopic corrections for surface and near-snow processes may still be needed.

Reconstructions of past climates based on isotope signals in polar snow have historically employed atmospheric IEMs coupled with isotopic-gradient smoothing inversion methods (e.g., Steen-Larsen et al., 2011; Masson-Delmotte et al., 2015). These studies assume that no other processes influence the isotopic signal.

1.4 The atmosphere-snow interface

There is a growing body of literature demonstrating that local processes such as wind-driven stratigraphy (Kochanski et al., 2018) and snow metamorphism (Colbeck, 1983) likely influence the isotopic content of surface (e.g., Münch et al., 2017; Wahl et al., 2021, 2022) and near-surface snow (Town, Warren, et al., 2008; Steen-Larsen et al., 2014; Casado et al., 2018; Madsen et al., 2019; Harris Stuart et al., 2023). It is uncontroversial to expect that post-depositional processes other than diffusion along isotopic gradients might modify the isotopic content of near-surface snow (e.g. < 1 m). However,

we argue that there is little agreement on the mechanisms or net impact of post-depositional change in seasonal or mean annual isotopic concentrations.

Modeling studies have shown that local meteorology can imprint near-surface atmospheric water vapor isotopic signals in the near-surface snow through forced-ventilation (i.e., wind pumping) (Waddington et al., 2002; Neumann & Waddington, 2004; Town, Warren, et al., 2008). Simulating the impacts of forced ventilation on snow requires time-resolved knowledge of the surface snow structure, surface winds, accumulation rate, and atmospheric and snow temperatures. Forced ventilation has been shown to potentially smooth *and* bias isotope records after deposition. The potential isotopic bias occurs in isotopically depleted winter layers during the relatively warmer summers at low accumulation sites (Town, Warren, et al., 2008). Accurate isotope-based climate reconstructions from ice cores may depend sensitively on time-resolved knowledge of local meteorological conditions (e.g., accumulation and temperature) because a changing climate may result in changing post-depositional biases Town, Warren, et al. (2008).

Observations confirm some results from the aforementioned modeling studies, but also present more questions. At Dome Fuji, Antarctica, a cold and low accumulation ice core site, there is a disconnect between the magnitude of the $\delta^{18}O$ annual cycle in precipitation and the firn (Fujita & Abe, 2006) that cannot be reconciled through inversion of Johnsen et al. (2000) isotope-gradient-driven diffusion. Mechanical mixing of surface snow also acts to smooth isotopic signals between precipitation layers. Horizontal averaging across wind-induced snow structures (e.g. Filhol & Sturm, 2015) causes large variability in environmental signals (i.e. stratigraphic noise, e.g. Steffensen, 1985; Münch et al., 2017; Zuhr et al., 2021, 2023). The surface snow and near-surface vapor water isotopes co-vary on an hourly-to-daily basis during summer in Northern Greenland (Steen-Larsen et al., 2014; Hughes et al., 2021; Wahl et al., 2021, 2022). Further observation and laboratory studies have shown that sublimation can cause an isotopic enrichment (Hughes et al., 2021).

Increased fidelity in surface and near-surface snow isotopologue observations have led to improved models of the same. Observed changes in surface snow $\delta^{18}O$ at East-GRIP has been successfully simulated by incorporating sublimation into an isotope-enabled surface energy budget model (Wahl et al., 2022). Ritter et al. (2016) and Casado et al. (2018) both employ elegant constrained models of the stable boundary layer. They ar-

gue that a thin layer of atmosphere over the Antarctic likely influences surface isotopic content resulting in enrichment of surface $\delta^{18}O$ at the expense of $\delta^{18}O$ vapor in the stable boundary layer. Windier sites will likely have a well-mixed boundary layer, resulting in correlation between surface $\delta^{18}O$ content and overlying $\delta^{18}O$ vapor content (e.g., Steen-Larsen et al., 2014; Wahl et al., 2022). Casado et al. (2021) show evidence of post-depositional change in surface snow induced by sublimation/deposition mechanisms, citing insolation and other surface energy budget processes as important to the surface $\delta^{18}O$ and d signals. At low accumulation sites scouring of annual layers is always a problem to contend with (e.g., Epstein et al., 1965; Casado et al., 2018).

On the other hand, snow pit data from across East Antarctica, a range of climates and accumulation rates, indicate that isotopic-gradient-driven diffusion, precipitation intermittency, and possibly spatial inhomogeneity may explain the signal to noise ratios at these sites and further mechanisms are not necessary (Münch et al., 2017; Laepple et al., 2018). At Summit Station, Greenland, Kopec et al. (2022) found very little post-depositional change in isotopic content of precipitation after deposition, yet argue that sublimation from the the Greenland ice sheet is responsible for the unique isotopic signatures observed in the precipitation. This is consistent with the idea that Summit Station has a high accumulation rate (24 cm/year l.w.e.) mitigating post-depositional modification, albeit a relatively warm mean annual temperature which would enhance post-depositional modification (Town, Warren, et al., 2008). Looking at one summer season at EastGRIP (Summer 2019), Zuhr et al. (2023) find evidence of local processes inducing post-depositional change in d in snow down to 10 cm, with the repeatability and potential causes remaining at large.

So, discrepancies in evidence and primary mechanisms of post-depositional modification of water isotope content of near-surface snow exist, inferred from both observations and models. Sublimation has already been shown to very likely the cause of observed changes in the top 0.5 cm of snow, but what is happening below this depth while the snow is still within the dynamic influence of the local atmosphere?

1.5 This study

To further quantitatively investigate the potential evolution of isotope signals below the surface snow layer (0-1 cm), we present observations from a time-resolved study

of near-surface snow (0-100 cm) from the EastGRIP site in Northeast Greenland (Mojtabavi et al., 2020). Short snow cores (i.e. snow profiles) (80-100 cm in length) were taken at primarily biweekly frequency during summers (May - August) for the 2017, 2018, and 2019 field seasons. Modeling indicates that significant change due to near-surface atmospheric influence is very unlikely below 1 m (Town, Warren, et al., 2008). The snow profiles were taken during the summer seasons when one would expect meteorology-induced post-depositional processes to be strongest in near-surface snow. The snow profiles overlap in depth from season-to-season, allowing a unique interannual look at the same snow layers. An age-depth model is developed for each individual snow profile to mitigate the impact of stratigraphic noise on grouping or averaging of isotope signals.

We will demonstrate that while there is inconsistent post-depositional modification of $\delta^{18}O$ during the summers and interannually, d shows more consistent modification in summer snow layers on weekly and interannual timescales. We explore the potential mechanisms causing these signals and implications of these results for future interpretations of d in polar snow, firn, and ice.

2 Site Description, Data, and Methods

The data and products presented here are all derived from observations at the EastGRIP ice core site located in the Northeast Greenland National Park. In Section 2.1 we present the meteorological context of our study. In Section 2.2 and Section 2.3 we present the surface snow isotope and snow profile isotope data sets, respectively. In Section 2.3.1, we explain the siting, extraction, handling, and processing of the snow profiles. In Section 2.4, we discuss the age-depth model applied to the snow profile isotope data set. In Section 2.5 we discuss nuances and caveats relevant to the interpretation of the data presented here. Table 1 contains an overview of the data used in this study.

2.1 Meteorology: data and context

The EastGRIP site sits at $75°37'47''N$, $35°59'22''W$, with an altitude of 2708 m (Mojtabavi et al., 2020), on fast moving ice stream (55 m/year Westhoff et al., 2022). There is a PROMICE weather station (Fausto et al., 2021) located approximately 300 m south of our study site. The site experiences a persistently high and directionally constant winds because its location on the ice sheet results in downslope (westerly) katabatic winds and west-

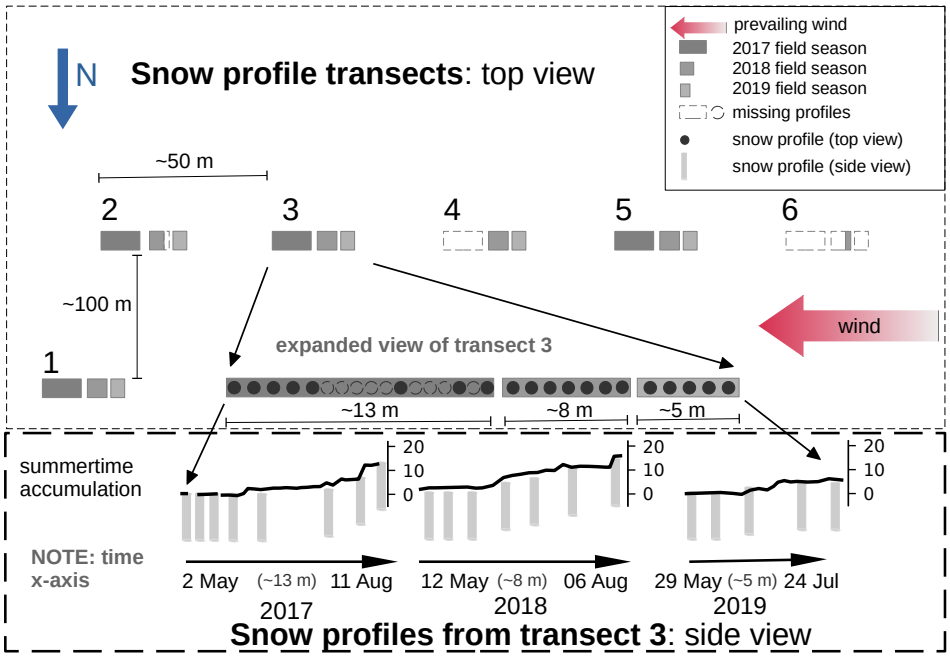

Figure 1: The top panel shows an overview of the relative spacing and timing of the transects along which the near-surface snow profiles were taken for this study. Each transect has the same snow profile pattern as illustrated in the expanded view of transect 3, a representative transect. The diagram is not to scale, but distances are noted. North is downward in this diagram. The prevailing wind direction is from the W-SW. The number and relative timing of snow profiles are accurately indicated. The bottom panel shows an illustration of the summertime accumulation along with snow profile timing. The study site is the EastGRIP ice core site in Northeast Greenland.

erly synoptic flow over the ice sheet (Putnins, 1970). See Table 1 for meteorology data summary.

The accumulation rate was measured as approximately 134-157 mm/year of liquid water equivalent (l.w.e.) from snow pit studies coincident with this work (Nakazawa et al., 2021; Komuro et al., 2021). Summertime daily accumulation was measured with stake lines during the 2016-2019 field seasons (Steen-Larsen, 2020a, 2020b; Harris Stuart et al., 2023). The stake line was 200-m long with 1-m spatial resolution in the 2016 field season, and 90-m long with 10-m spatial resolution for the remaining field seasons. We also determined changes in monthly mean snow height from PROMICE sonic ranger data (Fausto et al., 2021) for 2014-2019, with the annual snow accumulation rate being approximately 40 cm/year. The top 1-m of snow has a nearly constant density profile of approximately 337 kg/m^3, presumably constant because of the persistently high winds at EastGRIP (Schaller et al., 2016; Nakazawa et al., 2021; Komuro et al., 2021). The snow surface is spatially heterogeneous in height, with surface features smoothing slightly throughout the summer seasons (Zuhr et al., 2021, 2023).

2.2 Surface snow isotopes

The top 0-1 cm snow was collected along a 1000 m wind-parallel path in the 2016 field season, and a 100 m path for the 2017-2019 field seasons (Hörhold et al., 2023; Hörhold, Behrens, Hoffmann, et al., 2022; Hörhold et al., 2022; Hörhold, Behrens, Wahl, et al., 2022). During the 2016 and 2017 field seasons, samples from each site were collected and bagged individually, the measured $\delta^{18}O$ then averaged. During the 2017 field season, snow of equal amounts was also collected daily at the same locations then mixed into one sample bag. These were termed 'consolidated' samples. It was found from this work that the mean isotopic values of the individually bagged samples were the same as the less laboriously obtained 'consolidated' samples. Mean daily surface snow isotopic content for the summers of 2018 and 2019 were therefore determined from 'consolidated' samples.

Once collected, either individually or as a consolidated sample, the snow was sealed in an air-tight Whirl-Pak bag and kept frozen until measurement at the Alfred-Wegener-Institut in Bremerhaven, Gremany. Isotopic measurement procedures for surface snow are the same as for the snow profiles. See Section 2.3 for details.

2.3 Near-surface snow profile isotopes

2.3.1 Snow profiles: siting, extraction, handling, and measurement

The central data presented here are isotope measurements from a time-resolved array of 1-m near-surface snow profiles. See Figure 1 for a visualization of the snow profile sampling strategy. The snow profiles were taken along a transect progressing in the windward direction. On each sample date 4-5 snow profiles were taken, each one from a unique transect line. All profiles were extracted within a few hours of each other. The transect lines are spaced out by at least 50 m. We consider them independent representations of the near-surface snow as they are out of the range of isotopic spatial autocorrelation (Münch et al., 2016).

Snow profile locations along each transect were taken between three and twenty-one days apart, the most common sampling frequency being fourteen days. They were spaced apart by approximately one meter from sampling event to sampling event. Profiles taken along one track and adjacent in time are then considered to represent the same snow. These profiles are still susceptible to stratigraphic noise documented by Zuhr et al. (2023). A single profile was taken by gently pushing a 10-cm diameter carbon fiber tube (i.e. liner) with a 1-mm thick wall into the snow. Minimal compression of the snow column occurs during this process (maximum 2 cm, average 1 cm, Section 2.1 in Schaller et al., 2016). A small pit was cleared on the downwind side of the tube so that the liners could be carefully extracted will all snow. The resulting snow pit was then back-filled within two hours of the beginning of the process.

After extraction, each profile was quickly transported to a cold tent for cutting and storage. The profiles were cut at 1.1-cm resolution for the top 0-10 cm and 2.2-cm resolution for remainder of the profiles. Most profiles were not exactly 100 cm due to compression and a small amount of loss from the bottom of each profile. The snow was cut in an open-faced core tray using a 0.10-cm thick blade. Each sample was sealed in an air-tight Whirl-Pak bag and kept frozen until measurement at either the Alfred-Wegener-Institut in Bremerhaven, Deutschland or the Institute of Earth Sciences in Reykjavık, Island.

Measurements of $\delta^{18}O$ and δD concentrations were done using a Picarro cavity ring-down spectrometer (models L2120-i, L2130-i, L2140-i) and reported in per mil ($^{o}/_{oo}$) no-

tation as shown in equation 1 on the VSMOW/SLAP scale. Memory and drift corrections were applied using the procedure in (Van Geldern & Barth, 2012). The combined 1σ uncertainty in $\delta^{18}O$ is $0.11^{o}/_{oo}$ and for δD is $0.8^{o}/_{oo}$ for all isotopic measurements. We calculated the combined standard uncertainty (Magnusson et al., 2017) including the long-term uncertainty and bias of our laboratory by measuring a quality check standard in each measurement run and including the uncertainty of the certified standards.

2.4 Intercomparison of chronological layers

2.4.1 Depth correction

At EastGRIP, the uneven surface and concomitant heterogeneous distribution of precipitation results in spatially heterogeneous isotopic concentrations of snow (Zuhr et al., 2023). A perfectly horizontal average of $\delta^{18}O$ in snow then represents a mixture of events across time(Münch et al., 2017). Zuhr et al. (2023) estimates that the 2σ spread around mean $\delta^{18}O$ values as a function of depth is 2.9 $^{o}/_{oo}$ due to the impact of this stratigraphic noise. For this study, tracking chronological layers is critical so that wind-driven spatial heterogeneity in $\delta^{18}O$ is separated from other processes at work in the near-surface snow.

We applied a local depth correction to individual snow profiles to better compare chronological layers. Photogrammetric experiments at EastGRIP show that chronological layers of snow are inhomogeneous in thickness and spatial distribution (Zuhr et al., 2021), in agreement with prior efforts documenting wind-driven erosion and deposition in snow (e.g., Fisher et al., 1985; Colbeck, 1989; Filhol & Sturm, 2015). Important precipitation events will have uneven representation in the snow, and in extreme cases (high winds with low accumulation) entire annual layers could be scoured (e.g., Epstein et al., 1965; Casado et al., 2018).

For the 2017 snow profiles, we apply one depth correction to all profiles collected on one day. We use the mean change in height from the 200-m snow stake transect to adjust snow surface height relative to the first profiles of the season collected on 2 May 2017 (?, ?). We tracked changes in surface height along individual transects for the 2018 and 2019 seasons.

2.4.2 Age-depth model

The depth correction mitigates much of the stratigraphic noise induced by simple horizontal averaging, but not all. We developed an age-depth model for each individual snow profile to improve mitigation of stratigraphic noise on chronological layer intercomparison.

An illustration of the age-depth model process is shown in Figure 2. The end date for every profile is the extraction date. From this date we worked downwards in the snow and backwards in time, local maximum and minimum $\delta^{18}O$ values were found automatically. Dates were assigned to the $\delta^{18}O$ values are from the nearest maxima and minima in monthly mean temperature as measured at the nearby PROMICE weather station. We find at least two dates per annual layer.

The exact date assigned to each assignment for peak $\delta^{18}O$ and monthly mean temperatures was 31 July. M aximum temperatures occur consistently during mid-July at EastGRIP. Maxima in $\delta^{18}O$ have been observed to trail temperature maxima by as much as a month at EastGRIP (Harris Stuart et al., 2023) likely due to post-depositional sublimation, similar to Dome C, Antarctica (Casado et al., 2018) - a much lower accumulation site. The date assigned for the wintertime $\delta^{18}O$ minima was the first of each month. The Greenland Ice Sheet can experience moderately coreless winters (Putnins, 1970). So, the winter month with the minimum mean temperature may be one of a range of months (December-April).

The uncertainty in the age-depth model comes from a combination of the uncertainty in snow profile depth values and uncertainty in dates assigned to each $\delta^{18}O$ maxima or minima. Examining only uncertainty from the snow profile resolution, we assume that choice of the $\delta^{18}O$ maxima/minima values might be off by as much as one depth level in the snow profile. This is an error of ± 1 cm for the top 10 cm of each profile and ± 2 cm for the rest of each profile. If the accumulation rate is 40 cm/year then the resulting uncertainty in age-depth is approximately ± 9 for the top 10 cm and ± 18 days for the rest each profile.

We estimate the uncertainty in date assignment separately for Summar and Winter. Peak summer temperatures at EastGRIP consistently occur during the middle of July. Thus, the uncertainty in 31 July date assigned to peak $\delta^{18}O$ values is $\pm$ 7 days.

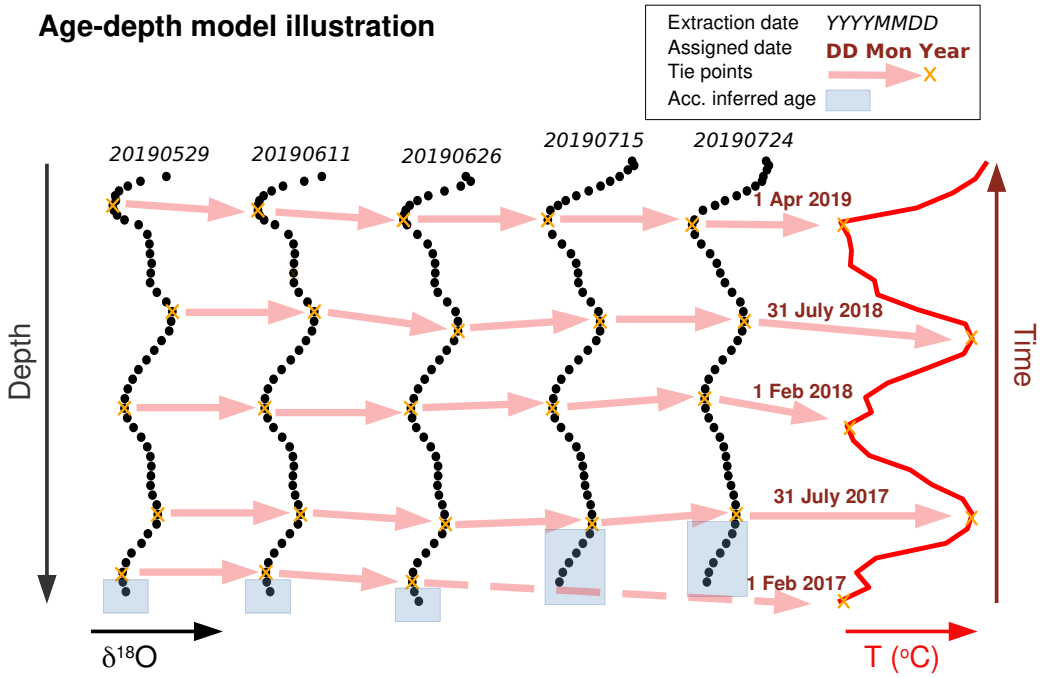

Figure 2: An illustration of the age-depth model applied to $\delta^{18}O$ data from transect 2 during the 2019 field season. The yellow stars represent automatically found peaks in $\delta^{18}O$ (black dots) and monthly mean 2-m temperature (red line). Each yellow star is assigned a date, and the intervening dates are linearly interpolated to a depth value. The lowest few $\delta^{18}O$ data points are assigned by an iterative process based on accumulation rate and manually checked. See text for details.

The coldest month in any winter may range from December to April (Putnins, 1970). Precipitation does not likely come during the minimum temperatures. The minimum $\delta^{18}O$ values then represent the coldest precipitation events. We assume that these coldest precipitation events happen during the coldest months. We know which months are coldest, but assigning a date to the coldest precipitation events overreaches the power of our meteorology data. So, we set the date for minimum $\delta^{18}O$ values to the first of each coldest month, acknowledging that we might be off by as much as ± 30 days.

Taken in total, we conservatively assess the 2σ uncertainty of each summertime date assignment as ± 25 days, and the uncertainty of each wintertime date assignment as ± 48 days. The accumulation rate at EastGRIP is not constant, with higher rates in Summer and Autumn than Winter and Spring. From the PROMICE sonic ranger data, approximately 50% of the accumulation comes from 20% of the events (Fausto et al., 2021). During high accumulation rate time periods, the dating uncertainty will be much smaller, and vice versa.

Figure 2 represents a transect in which the age-depth model did not vary much from profile-to-profile. In this case, the depth correction provided a strong start for the age-depth model. The age-depth model varies more between snow profiles taken during the 2017 season when the depth correction was not as strong. Evidence for this can be seen in the dramatic difference in uncertainty around the 2017 mean profiles between Figure 3(a) and Figure 3(c).

The age-depth model is reliable when clear $\delta^{18}O$ maxima and minima exist in the snow profiles, which is true for the vast majority of each profile. The exceptions are systematically at the bottom of each snow profile. Rarely did the bottom of any core end in a clear maxima or minima, so a different procedure was developed for these occurrences. First we use the earliest date assigned (i.e. deepest maxima or minima) in the profile to estimate the remaining snow left undated. We then iteratively found the mean accumulation rate for this remaining snow by assuming a mean accumulation rate of 40 cm/year to frame the appropriate time period then determining the mean accumulation rate for the correct time period using the sonic ranger data set from Fausto et al. (2021). The age-depth model for the bottom of the profile is the inverse of the mean accumulation rate. Finally, we assessed the resulting $\delta^{18}O$ profile against the entire data set. Profiles with dramatically different age-depth models at the bottom were assigned a starting date

to match their $\delta^{18}O$ values with seasonally appropriate times. Between 10-20% of each profile will have received the accumulation-rate-informed age-depth model.

2.5 Nuances and caveats in the snow isotope data set

2.5.1 Decorrelation distances and snow profile comparisons

Our sampling strategy is designed to separate spatial and temporal variability of isotopic content of the near-surface snow. The sampling strategy is inherently destructive. This results in trade-offs between accurate sampling and monitoring temporal variability. The transects shown in Figure 1 observe the same location as much as possible by sampling at approximately 1-m spacing along each transect. The 1-m spacing keeps each profile well within established spatial decorrelation distances for spatially successive water isotope samples (1.5 m) in similar climates (Münch et al., 2016). We did not sample much closer than 1-m to leave the next sample relatively undisturbed. This last point is further explored in the next section (Section 2.5.2).

The decorrelation distances derived in Münch et al. (2016) were done so without application of spatial depth adjustment or an age-depth model to align chronological layers. They thus represents extreme decorrelation distances for our data set. We expect our decorrelation distances to be slightly higher after the application of depth adjustments, and much higher after application of our age-depth model.

While each transect line is intended to represent the same snow, during 2017 many (18) profiles were taken along each transect although not all used here (only 8). Even considering the enhanced autocorrelation of samples because of our age-depth model, it is very likely that the snow extracted from a transect at the beginning of the 2017 season does not represent the same location as the snow from the end of the 2017 season along the same transect. We consider this later when examining intraseasonal evolution of the near-surface snow.

The transect lines are separated by 50 m or more to provide 'independent' representations of the snow surface. Several dune and sastrugi features will manifest in these distances (Zuhr et al., 2021), making each of these transects independent as far as precipitation and wind-driven surface features are concerned.

2.5.2 Mitigated biases due to sampling

The combination of a 1-m distance between each profile along one transect along with prompt back-filling of each extraction mitigates the influence of near-surface meteorology on the next upwind profile. High temperature gradients take days to weeks to propagate through the snow these distances (Town, Waddington, et al., 2008). The potential influence of force ventilation on near-surface snow due to tapers off dramatically after about 50 cm (Town, Warren, et al., 2008). So, our sampling procedure prevents unintended post-depositional change due to extra exposure to the near-surface atmosphere.

2.5.3 Missing data and other sources of uncertainty

Transect line 4 was impacted by traffic or resampling during the 2017 field season. It was left out of these analysis. Transect lines 2-5 were shifted inadvertently up one transect in the middle of the 2018 field season due to a change in field personnel. This was corrected during post-processing.

In addition to the 1-m profiles used here, nine shorter profiles (30 cm in length) were taken in 2017. We do not use these data here as they do not provide interannual information. The shorter profiles nevertheless represent distance traveled along each transect. For the short profiles, the spacing between profiles was smaller, approximately 50 cm. So, the total distance traveled along the 2017 transects is estimated as a conservative 13 m.

Compression often occurred during the extraction of the snow. Standard procedure would be to apply a correction for this compression evenly across each profile, particularly in deeper firn or ice. However, we believe that the location of compression is more likely localized in near-surface snow. In a 1-m snow profile from this site, there are least five locations where the compression might have occurred, at the surface or the Spring or Autumn hoar layers. It is also certain that the compression did not occur evenly across any profile. The compression values are small relative to the profile lengths and identifying the hoar layers after extraction is tricky. So, we leave the compression amount as an effective uncertainty in the dating, a probable maximum value of 9 days.

Finally, we did not adequately assess the relative starting heights of the transects at the beginning of each season. This induces relative errors of around 3-5 cm in our depth

adjustment between each snow profile based on May surface roughness estimates from (Zuhr et al., 2021). The missing information does not impact the age-depth model.

3 Results

The snow sampling strategy employed here is designed to provide successive seasonal and interannual looks at snow layers to track any post-depositional isotopic changes as the snow ages. The surface snow data (0-1 cm) is only from summer. It is not precipitation, but provides an immediate context for the isotopic content of recent snow accumulation. The near-surface snow (0-100 cm) we characterize with annually returning, closely-spaced snow profiles along distributed transects. This strategy allows snow profiles to be meaningfully intercompared on a weekly-to-biweekly basis throughout a summer season. The sample depth ensures that we have measured past the lower boundary of any potential influence of the near-surface atmosphere (e.g., Waddington et al., 2002; Town, Warren, et al., 2008), and provides successive looks at the same snow layers as they age from year-to-year. The interannual data are presented in Section 3.1 and summer-only data are presented in Section 3.2. The implications of these results and future work are discussed in Section 4.

3.1 Interannual variability and evolution

Figures 3 and 4 show annually successive surface and near-surface snow isotopic content for $\delta^{18}O$ and d, respectively. The dates represented by the snow span 2014-2019. The age of the snow may range from two to three years depending on the extraction date. Figures 3(a) and 4(a) show the mean profiles with $2\sigma_{\bar{x}}$ shading around each mean. The data are plotted against relative depth with 0 m chosen as 29 May 2019, the day of the first snow profile during the 2019 summer field season. Figures 3(b) and 4(b) show the difference between each profile as a function of relative depth. These difference profiles represent the isotopic change due to aging in the firn.

As stated in Section 2.4, we have mitigated the impact of stratigraphic spatial inhomogeneity on horizontal averaging (Figures 3(a,c) and 4(a,c)). For the 2017 profiles, we apply the same depth correction to all snow profiles as individual surface height tracking was not possible. This results in larger $2\sigma_{\bar{x}}$ shading around the 2017 mean snow profiles.

Figures 3(c,d) and 4(c,d) show the same isotopic data as in their respective panels (a,b), but now against the age-depth model described in Section 2.4. The age-depth model better aligns chronological layers than the accumulation adjustments, further mitigating deleterious impacts of spatial inhomogeneity in stratigraphy and densification on quantitative comparison $\delta^{18}O$ and d in snow layers. This can be seen in a decrease $2\sigma_{\bar{x}}$ values from panel (a) to panel (c) in Figures 3 and 4, particularly for the 2017 snow profiles. Although accumulation is fairly continuous at EastGRIP (Fausto et al., 2021), more accumulation comes in the Summer and Autumn over Winter and Spring. This weighting difference weighting explains the differences between Figures 3(b)/4(b) and 3(d)/4(d).

Figure 5 shows the difference between annually successive mean snow profiles. It is similar to panel (d) from Figures 3(c,d) and 4 but with $2\sigma_{\bar{x}}$ shading. Figure 5 can be interpreted as how $\delta^{18}O$ and d evolve one or two years after being interred, now as a function of reference snow profile age.

Annual and seasonal statistics from Figures 3, 4, and 5 are shown in Tables A1-A4 in Appendix A.

3.1.1 Interannual evolution of $\delta^{18}O$

Mean annual $\delta^{18}O$ values are fairly constant throughout this time period regardless of aging, approximately -36 $^{o}/_{oo}$. However, there is significant variability in the peak summer $\delta^{18}O$ in each profile, regardless of snow age. The 2019 summer has the greatest peak $\delta^{18}O$ values. There is not concomitant variability in the minimum winter $\delta^{18}O$ values in this record. Some differences between profiles seem significant when plotted against relative depth. However, when the age-depth model is applied, differences between profiles show no significant interannual change in $\delta^{18}O$ (Figures 3(d) and 5(a)).

We compute a seasonal temperature sensitivity (γ_t) using minimum (winter) and maximum (summer) $\delta^{18}O$ values with corresponding minimum and maximum monthly mean temperatures, using the same tie points as those used in the development of the age-depth model (Figure 2). This is similar to subseasonal temperature sensitivities found in Greenland (e.g., Shuman et al., 1995; Bolzan & Pohjola, 2000) and the Antarctic (e.g., Casado et al., 2018). We find γ_t for each half year by using the ratio of seasonal change (summer-to-winter, winter-to-summer) in $\delta^{18}O$ over the seasonal change in monthly mean temperature. We find a mean γ_t that starts at approximately $0.297 \pm 0.03 ^{o}/_{oo} \cdot {}^{o}C^{-1}$ and

decreases at a rate of $0.096 \pm 0.04 {}^{o}/_{oo} \cdot {}^{o}C^{-1} \cdot year^{-1}$. We have chosen to fit a linear pattern, but there could be a more dramatic drop in γ_t over the first 0.5 years then a much slower change in γ_t thereafter. More data and modeling are necessary to probe this relationship for EastGRIP.

During the season of extraction, the surface snow $\delta^{18}O$ values (purple squares) and mean summer snow profile $\delta^{18}O$ values match in mean and approximate variability for this record. After aging one year, the mean snow profile $\delta^{18}O$ for July 2018 extracted in 2019 matches the mean surface snow $\delta^{18}O$. However, the surface snow $\delta^{18}O$ from 2016 and 2017 are several per mille enriched over the snow that has aged one or two years.

Using the summer $\delta^{18}O$ profile peaks as annual markers, we find a mean annual accumulation rate of 45.6±3.8 cm (13.5±1.1 cm/year l.w.e.) for this time period. This is consistent with accumulation rates for EastGRIP just prior to the observation period with a similar method (Nakazawa et al., 2021; Komuro et al., 2021), as well as coincident estimates from PROMICE sonic rangers (Fausto et al., 2021).

3.1.2 Interannual evolution of deuterium excess

Figure 4 shows the interannual variability of deuterium excess (d). Clear seasonal cycles are shown on both depth and age-depth scales. The minima occur during the Spring and Summer, while the maxima occur during Autumn as one might expect from Johnsen and White (1989), but in variance with Kopec et al. (2022). There are significant differences between the summer d values from surface snow and the snow profiles during the season of extraction. The mean summer surface snow d is 8-10 ${}^{o}/_{oo}$, whereas the mean snow profiles show d values of only a 3 and 5 ${}^{o}/_{oo}$ in 2018 and 2019, respectively. This is similar to what was found by Zuhr et al. (2023) for summer 2019 at EastGRIP. In 2017, we see higher mean d in the summer snow profiles just after deposition, but still less than in the mean surface snow d (See Table A5). The surface snow has a large range in d values as synoptic events bring in high d precipitation, followed by periods of decreases in d due to sublimation (Harris Stuart et al., 2023). The evolution of the near-surface snow during the summer field seasons is discussed in greater depth in Section 3.2 and Section 4.

The differences between d profiles shows a distinct pattern peaking during the summer layers (Figures 4(d) and 5(b)). The surface summer snow starts with a relatively high d value that decreases by as much as 5 ${}^{o}/_{oo}$ by the time it is extracted as a snow

profile. After aging for one or two years, the same summer layer d have increased up to 5 $^{o}/_{oo}$because the Autumn maximum peaks broaden into Summer and Spring layers. Although not rising to the level of $2\sigma_{\bar{x}}$ significance, there is also a persistent decrease is winter d values shown in Figure 4(d) as the snow ages interannually. The mean annual values of d do not change from year-to-year, regardless of aging (Table A3).

3.2 Summer evolution of $\delta^{18}O$ and d

Figure 6 provides a look at the isotopic evolution of the near-surface snow during the summer field seasons. The extraction dates (upward arrows), 2-m air temperature, and accumulation from bamboo stake field are provided for context. Some spatial variability is no doubt represented in contour plots as temporal variability although snow profiles along one transect were nearly coincident in space and corrected for changes in surface height (Figures 6(d-i)). Each upward arrow represents the mean of 4-5 snow profiles from different transects. The spatial variability is likely averaged out by grouping of snow profiles from different transects.

We show little more than the first annual cycle (0-50 cm) because there is no detectable subseasonal change below approximately 20-30 cm. However, the top 10-15 cm of snow shows important evolution responding to both influxes of new accumulation and impacts of sublimation during periods of high temperatures and low-to-no accumulation. New accumulation can bring in a range of $\delta^{18}O$ values, but typically has a high ($\geq$10 $^{o}/_{oo}$) d content. During periods of low-to-no accumulation there are coincident increases in $\delta^{18}O$ and decreases in d. This is a known signal of sublimation (Hughes et al., 2021; Wahl et al., 2022; Harris Stuart et al., 2023), yet the patterns could be a result of spatial inhomogeneity represented as temporal evolution. We find this unlikely due to the consistency with which sublimation signals happen during low-to-no accumulation using time as the x-axis perspective. Further, low-to-no accumulation periods do not show other combinations of changes in $\delta^{18}O$ and d, and each contour plot represents an average across spatially distant transects.

Figures 7-9 illustrate the changes in mean daily profiles from two dates from the middle of each summer during low-to-no accumulation. Significant increases ($p < 0.05$) in $\delta^{18}O$ are seen the summers of 2017 and 2019, down to 10-15 cm. Coincident decreases in d are also seen in these difference plots, but not to $p < 0.05$. Temporal changes in

the 2018 snow profiles are not so easily encapsulated in a profile difference plot shown. In this case there is no significant change in $\delta^{18}O$ and d over the chosen low-to-no accumulation period. Other periods during 2018 may show significant differences in their profiles, but we choose here to keep the time periods as similar as possible for this illustration.

Nevertheless, across the 2018 and 2019 summer seasons we see a 5 $^{o}/_{oo}$ difference in d from when it is sampled at the surface and when it is extracted as a snow profile in the same summer. This is difference is not apparent in the 2017 summer data. See Figure 4(d) and Table A5 in the Appendix.

4 Discussion

There are significant changes in the isotopic content of near-surface snow after deposition at the EastGRIP site. We observe these changes happening on two timescales, during the summer season and interannually. The largest changes we observe are in the summer snow layers on both timescales. Enrichment in $\delta^{18}O$ and a decrease in d can happen during the summer season in the top 10-15 cm of snow during low-to-no accumulation periods. A subsequent increase in the summer snow layer d occurs as the snow ages one or two years in the firn. Below we discuss potential mechanisms for these processes, their implications, and make recommendations for future work.

4.1 Mechanisms of post-depositional processes at EastGRIP

The factors that combine to change isotopic content of near-surface snow are: elevated air and snow temperatures, air and snow temperature gradients, absolute humidity levels, air and snow humidity gradients, near-surface wind speeds, surface structure, snow density, accumulation rate, and redistribution (scouring and filling) of snow. As an observational effort, inferences we make about potential mechanisms necessarily require further study, recommendations for which we make in Section 4.2. Nevertheless, some strong inferences can be made through context and compositing of the results from Section 3.

4.1.1 Summer

As stated in Section 3.2, the change in near-surface $\delta^{18}O$ and d that occurs during summer can have a sublimation signature, increase in $\delta^{18}O$ and decrease in d, during low-to-no accumulation events. This has also been observed and modeled at East-GRIP in surface snow (Wahl et al., 2022). Similar patterns of isotopic change were observed in a higher resolution, vertically and horizontally, summertime data set for East-GRIP down to 30 cm (Zuhr et al., 2023).

The mean surface snow d in this data set is almost always greater than the snow profile d that has aged a few days or weeks (Figure 4(c)), which is a likely sublimation signal. However, there is not proportional enrichment of $\delta^{18}O$ when comparing surface snow to snow profiles (Figure 3(c)). The isotopic changes we see in our case studies (Figures 7-9) do not always rise to the level of $2\sigma_{\bar{x}}$ significance, likely induced by spatial inhomogeneity. Clear patterns related to possible post-depositional modification do seem present when looking at the summers as a whole (Figure 6).

Exploring possible mechanisms for the clear differences we see in d between surface snow and near-surface snow, as well as the patterns shown in Figure 6, we first assess isotopic gradient diffusion (Johnsen et al., 2000). Using Johnsen et al. (2000) isotopic-gradient-driven diffusion under extreme conditions (i.e. the steepest mean isotopic gradients, warm summer temperatures -11 ^{o}C for 60 days), there can be a change in $\delta^{18}O$ of up to 2 $^{o}/_{oo}$. We observe in our snow profiles changes much larger than 2 $^{o}/_{oo}$ over 47 days in 2017 (Figure 7(a)). We are not observing a pure isotopic-gradient diffusion situation because the real snow surface is open to the atmosphere, its isotopic content fluctuating on many time scales. Casado et al. (2021) show that summer surface snow $\delta^{18}O$ at Dome C, Antarctica responds to more than surface temperature, with sublimation and deposition being important aspects to simulating isotope observations.

The Johnsen et al. (2000) diffusion also has a smoothing effect, but we also observe biases induced in the surface and near-surface snow. A change in mean isotopic content over a shallow, near-surface layer implies the influence of the near-surface atmosphere. To substantiate this inference, we simulate interstitial air flow with a model of wind-pumping in snow (Colbeck, 1997). We use mild surface topography and mean wind conditions (rolling dunes, $\lambda = 0.5$ m, $h = 0.25$ m; $\rho_{snow} = 350\ kg/m^3$; wind speed = 5 m/s). The surface topography is idealized, but similar to that documented by Zuhr et al. (2021, 2023). We

find that air flow can be as much as a few cm/s down to 10 cm in the snow, making influence of the near-surface atmosphere on a shallow, near-surface layer of snow possible. On the other hand, laboratory experiments by (Ebner et al., 2017) show that forced ventilation of snow almost certainly causes hand-to-hand exchange within the snow, rather than inducing transport of atmospheric water vapor directly down to different depths as was modeled in Town, Warren, et al. (2008). Combining these ideas, enhanced exchange between the ventilated layers during the summer seems plausible, causing a *net* sublimation isotopic signal in a 10-15 cm layer of near-surface snow during summertime low-to-no accumulation events at EastGRIP. This is not observed in every season in our record, which points toward more complicated processes likely related to snow redistribution and the surface energy budget.

The stratigraphy at EastGRIP documented by Zuhr et al. (2021) is a potential source of temporal isotopic variability when redistribution of settled snow occures. This is considered a dominant source of spatial stratigraphic noise in isotopic signals in low accumulation areas such as EastGRIP (e.g., Münch et al., 2017). The heterogenous snow surface structures generated during polar winters have been observed to smooth during subsequent summers (e.g., Gow, 1965; Albert, 2002). Zuhr et al. (2021) observed a smoothing of the rough snow surface throughout the summer season at EastGRIP, with small negative correlation between variance in surface structure and local winds. The implication here is that scoured areas can fill during precipitation with light-to-moderate winds. During low-to-no accumulation periods like those in focus here other filling mechanisms are also important.

Smoothing of sastrugi under relatively moderate winds during summer months at the South Pole has been explained by heating of sastrugi flanks while the Sun spirals around the horizon. Frost is deposited on the backs of dunes and sastrugi under extended periods of clear skies and high temperature inversions (Gow, 1965). Filling of scoured areas results afterwards when the fragile surface facets are toppled by winds of mild or moderate intensity. We have witnessed this combined mechanism at EastGRIP. We infer that under common conditions at EastGRIP redistributed snow can have a sublimation/deposition signal. Modeling by Casado et al. (2021) indicates this process could decrease $\delta^{18}O$ and increase d. We presume this mechanism results in a net mass deposition at the surface. Important questions remain here:

- In what proportion does the mass come from the near-surface atmosphere or snow under these conditions?
- To what extent does this mechanism occur, either in frequency or in mass transfer?

Looking ahead, a clear-sighted experiment around frost formation would couple snow and near-surface atmosphere temperature and humidity measurements, as well as their gradients, with time-resolved snow density and isotopic measurements to simulate where the frost mass is coming from. It may be that if mass transfer from subsurface layers is not directly detectable, it can be inferred isotopically.

Of course, accumulation provides a fundamental contribution to the isotopic signal of snow. In the context of post-depositional processes, a high accumulation rate will advect snow away from the influence of the near-surface atmosphere quickly (e.g., Town, Warren, et al., 2008). In 2018, there is almost 20 cm of accumulation during our observation period, which removes the late Spring/early Summer from the influence of the near-surface summer atmosphere according to our analysis.

The observations presented here are complicated enough that a more comprehensive approach is necessary to clearly distill the processes at work and their relative importance during the polar summer. Such an approach would in cloud amount, isotopic content, and frequency of precipitation and redistributed snow, as well as magnitude and variability of latent heat fluxes. We make recommendations in Section 4.2 to this effect.

4.1.2 Interannual

There does not seem to be clear interannual changes in $\delta^{18}O$ between the mean profiles presented above. Using the same isotopic-gradient diffusion scenario as in Section 4.1.1 we simulate ${}^{\Delta\delta^{18}O}/_{\Delta T}$ can change at a rate of 0.16 ± 0.03 ${}^{o}/_{oo} \cdot {}^{o}C^{-1} \cdot year^{-1}$ ($p < 0.05$), effectively the same rate we observe in our data. However, the mean d signal in summer snow experiences an increase of up to 5 ${}^{o}/_{oo}$ after one year in the snow (Figure 5) due to a shifting and broadening of the Autumn d peak. Although this almost the same magnitude of a sublimation-induced decrease in d that *can* happen through a low-accumulation summer season, we believe these processes are not explicitly linked.

The shift in d peak can be partially explained by (Johnsen et al., 2000) isotopic-gradient-driven diffusion. Our simulations of an annual cycle of isotopic-gradient-driven diffusion on the mean 2019 $\delta^{18}O$ and δD profiles result in a broadening and a downward (backward in time) shifting of the Autumn d peak (See Appendix, Figure B1). This Autumn peak broadening in d results in a d increase of 2-5 $^{o}/_{oo}$ in the summer snow layers, similar to our observations. What is also present in the simulations, but missing from the observations, is an adjacent negative excursion in d in the previous spring snow layer. The isotopic-gradient diffusion smooths signals, resulting in no net bias. The snow profile observations show a bias induced in d. Sensitivity tests find that applying the diffusion simulations to smoother mean profiles as opposed to individual profiles with sharper features underestimates the amount of isotopic-gradient diffusion. A more mechanistic study is necessary here resolve specific processes at work and better understand the smoothing and potential biases.

The increase in summer layer d most likely occurs during the following Autumn when snow temperatures are still relatively high and snow temperature gradients are also very high (e.g., Town, Waddington, et al., 2008). The summer layers during their first year in the snow have a $\delta^{18}O$ vs δD slope of 7.87 $\delta D/\delta^{18}O$, which changes to 8.56 $^{o}/_{oo}\cdot$ $^{o}/_{oo}{}^{-1}$ after one year in the snow (Table A6). This represents dramatic resetting of the meteoric water line relationship after advection away from the direct influence of the near-surface atmosphere. We suggest a mechanism of temperature-gradient-driven interstitial vapor diffusion. Even though interstitial air flow will be low as these summer layers are advected downwards, there are still large synoptically and seasonally driven temperature gradients in the snow down to 50 cm (Town, Waddington, et al., 2008). Relatively high temperature gradients and increasing temperatures also occur during late Spring. At EastGRIP, a summer snow layer that has been buried for three-quarters of a year will be almost 30 cm away from the surface. So, we consider Spring a less likely candidate for timing of d increase as the synoptic and seasonal temperature gradients rapidly decrease in strength when moving away from the surface snow (Town, Warren, et al., 2008).

These results are fairly independent of the age-depth model because the model formulation first relies on tying together like features in the $\delta^{18}O$ profiles first, then assigning a specific date to each $\delta^{18}O$ feature. Shifts d peaks are then understood as shifts in

δD relative to $\delta^{18}O$, as expected due to the different diffusion coefficients (Hellmann & Harvey, 2020), irrespective of the dates assigned to a given profile depth.

4.2 Implications and Future Work

We find that d can undergo significant post-depositional change both during a summer season and over one-to-two years in the firn. Summer precipitation that falls at East-GRIP with elevated d values can experience a sublimation-induced decrease just after deposition, and then a subsequent increase likely due to vapor-pressure-gradient induced post-depositional change deeper in the firn. It seems that d not only has information about source region and transport history, but also integrates the local near-surface snow history at sites where meteorologically-induced post-depositional isotopic change in near surface snow occurs. In these data, mean summer layer d decreases by up to 5 $^{o}/_{oo}$ due to sublimation prior to being advected away from the direct influence of the near-surface atmosphere. Prior literature indicates the largest post-depostional change occurs at sites characterized by a combination of relatively low accumulation, relatively high surface temperatures and vapor pressures, high winds, and high surface relief (Waddington et al., 2002; Neumann & Waddington, 2004; Town, Warren, et al., 2008). The specific combination of these factors for a given site requires process-based models of the near-surface snow to be coupled with IEMs for proper characterization.

We show that significant enrichment of $\delta^{18}O$ can happen in the near-surface snow after deposition during summertime low-to-no accumulation events. This is likely due to sublimation, consistent with previous observations and modeling for surface snow at EastGRIP (Wahl et al., 2022). The $\delta^{18}O$ content of snow is often used as a regional temperature proxy, whether local atmospheric temperature or cloud temperature, because of aforementioned strong spatial and temporal relationships between $\delta^{18}O$ and temperature. However, our results in the context of broader literature base (e.g., Casado et al., 2021; Wahl et al., 2022) indicate that the $\delta^{18}O$ is probably much better interpreted as a surface energy budget proxy, or a combined temperature and latent heat flux proxy.

A more nuanced interpretation of the $\delta^{18}O$, or δD, proxy is particularly important to studies like Jones et al. (2023), who interpret summer-only δD changes in West Antarctica as changes in summer temperature due to changes in insolation. Interpreting changes in δD as both changes in temperature and latent heat flux could help explain why the

West Antarctic summer δD pattern is correlated with Milankovitch insolation patterns even though annually coincident winter correlation in δD is not clearly evident. Similarly, studies using $\delta^{18}O$ as summer or annual temperature proxies in ice sheet elevation reconstructions may be biased warm due to influence of sublimation on $\delta^{18}O$ (e.g., P. M. Grootes & Stuiver, 1987; Lecavalier et al., 2013; Badgeley et al., 2022), likely yielding a thinner ice sheets than were actually present.

Isotope-enabled GCMs (Werner et al., 2011) and cloud physics schemes (e.g., Petit et al., 1991; Ciais & Jouzel, 1994; Dütsch et al., 2019) designed to leverage the d parameter over the polar regions are routinely trained on polar surface snow or deep ice cores. These efforts may be at risk of heuristically incorporating post-depositional processes into their cloud physics or super saturation schemes. Similarly, a recent definition of d optimized for cold climates used surface snow as ground truth without assessment of the surface snow's d vulnerability to post-depositional change (Uemura et al., 2012).

Changes in near-surface snow due to the influence of the atmosphere or temperature gradients in the snow are possible at any time of the year. Our data set can primarily tell us about the changes in summer snow layers during summertime and interannually. When we extract snow, the timing of accumulation to advect snow away from the surface, and seasonal temperature and humidity are part of our detection bias. We expect most isotopic change to occur during summer and warm periods during shoulder seasons due to higher vapor pressures and vapor pressure gradients in the atmosphere and near-surface snow. Vapor-pressure-gradient-induced post-depositional change may occur in other seasons soon after deposition, but we are not able to detect this due to extraction timing. For example, we see that the near-surface atmosphere has influence at EastGRIP down to 10-15 cm where the accumulation rate is 40 cm/year (Figures 6-9). In this case, it is possible that snow from a low-accumulation Spring may undergo post-depositional isotopic change during a subsequent Summer.

To better interpret $\delta^{18}O$ and d as proxies for climate, we see the need for improved field experimentation to characterize seasonally-dependent post-depositional change. This would manifest as longer sampling periods, possibly annual in duration, over a period of years to document the scope of post-depositional change at a range of sites vulnerable to post-depositional change. Data sets such as these would help our second recommendation: further development of streamlined, site-agnostic process-based models that

include the impact of the surface energy budget, near-surface snow vapor dynamics, and redistribution processes on the isotopic content of near-surface snow (e.g., Town, Warren, et al., 2008; Touzeau et al., 2018; Stevens et al., 2020; Kahle et al., 2021; Hughes et al., 2021; Casado et al., 2021; Wahl et al., 2022). This combination will allow for training of model parameters and investigation into compensating impacts of all potential processes impacting post-depositional isotopic change of near-surface snow. Coupling of the near-surface models with existing meteorological and climate IEMs will have the potential to refine all reconstructions of past climate based on water isotopic content of polar ice cores.

4.3 Conclusions

Water isotopes in polar snow have historically been used to infer information about past climates of polar ice sheets, as well as the integrated history of polar precipitation. These inferences rely on a continuous physical understanding of the water's history, from source to extraction. A weak link in this understanding exists in the near-surface polar snow where dynamic snow metamorphism occurs under the influence of local meteorology and climate. This data set provides successive looks at the same snow layers, allowing us to document how the near-surface snow ages isotopically on two timescales, during summer and interannually. We use surface and near-surface snow extracted from the EastGRIP site in NE Greenland during summer months of 2017-2019 to help address this gap in understanding, as such our conclusions about the summer layers are strongest.

Near-surface snow collected during the same summer season shows isotopic signatures of sublimation down to 10-15 cm as the snow ages during low-to-no accumulation events. This depth is consistent with the depths of wind-pumping likely present at EastGRIP, indicating the potential influence of the near-surface atmosphere. The combined $\delta^{18}O$ and d sublimation signature is inconsistent from season-to-season, pointing to the need for more process-based understanding. The mean summer surface snow d is always greater than the mean d from snow profiles extracted later in the season, indicating sublimation through the summer season. It is possible that similar changes are occurring shortly after deposition in other seasons at relatively warm or low accumulation sites, particularly during early Autumn and late Spring.

We see significant increases in d of up to 5 $^{o}/_{oo}$ in the summer layers after one-to-two years of aging in the firn. We see decreases in d in other seasonal layers, but these decreases do not rise to the level of $p < 0.05$. The increases we observe in summer layer d are coincidentally almost the same the magnitude as the decrease in d observed during some summer seasons immediately after deposition. No coincident interannual change in $\delta^{18}O$ is observable in our data. There is a significant decrease in seasonal $^{\Delta\delta^{18}O}/_{\Delta T}$ over our study period, but more work is necessary to determine the pattern and rate of this change.

Mechanisms for the changes during summer months include a combination of isotopic-gradient-driven diffusion and wind-enhanced net sublimation from the near-surface snow. We postulate that some summer wind-driven redistribution events can have distinct sublimation/deposition signatures after surface faceting events. Interannually, isotopic-gradient diffusion can explain the changes in seasonal isotope-temperature sensitivity. It also explains some but not all of the Δd pattern we observe. We suspect seasonally- and synoptically-induced vapor-pressure gradients in the near-surface snow to be an important metamorphic process during Spring, Summer, and Autumn months. They ought to be less important during Winter months due to the low interstitial vapor pressures.

Our observations are relevant for the interpretation of water isotopes as proxies for past climates in polar regions. Intermittent summer enrichment of surface and near-surface $\delta^{18}O$ indicates that this proxy should likely be interpreted as an integrated local cloud or surface temperature *and* near-surface latent heat budget proxy. Similarly, the summer and interannual evolution of d shown here indicates that d is not only a proxy for water source region conditions and transport history, but also integrates local meteorology and climate information in the months and years after deposition - at least in summer snow layers.

Our results are complicated by the extractive nature of the observations, where spatial variability is at risk of being interpreted as temporal variability. Our strategic spatially-distributed sampling program coupled with the depth corrections and an age-depth model puts most of the stratigraphic noise in our error bars, but of course not all.

Our results are specific to the present day climate at EastGRIP, a relatively warm but low accumulation site on the Greenland Ice Sheet. These results are consistent with prior work exploring and documenting post-depositional processes (e.g. Waddington et

al., 2002; Neumann et al., 2005; Town, Warren, et al., 2008; Steen-Larsen et al., 2014; Casado et al., 2021; Hughes et al., 2021; Wahl et al., 2021), and demonstrate that more general revisions to interpretations of water isotope proxies in polar snow are needed. Questions remain about potential changes in other seasons, as well as the mechanisms at work and their relative importance. We also still lack generalized tools for assessing near-surface post-depositional modification of water isotope proxies at ice core sites, which are critical for interpretation of water-isotope-based climate records.

We recommend further field work documenting the annual evolution of the near-surface snow with successive snow profiles overlapping in their depth, but also assessing spatial variability. These data, an extension of those presented here, will act as a training ground for the development of isotope-enabled, process-based models of the near-surface snow. Driving, or coupling, the near-surface snow models with meteorological IEMs will greatly advance site-agnostic means for interpretation of past climates using polar snow.

Appendix A Tables of snow profile statistics

We provide tables of statistics for the snow profiles and their changes presented in Figures 3(c,d) and 4(c,d) composited by season or year.

Appendix B Supporting simulations

B1 Isotope-gradient-driven diffusion simulations

We use the Johnsen et al. (2000) isotopic-gradient-driven diffusion model to assess the potential impact of this mechanism to explain the pattern and magnitude of the changes we observe in the near-surface snow at EastGRIP. The model is run on the mean $\delta^{18}O$ and δD profiles from the 2019 field season using the following scenario that roughly approximates the seasonal cycle at EastGRIP: Summer is 60 days with snow at -11^oC, Autumn is 60 days with snow at -28.5^oC, Winter is 180 days with snow at -40^oC, Spring is 60 days with snow at -28.5^oC. This scenario is realistic, but will overestimate the amount of diffusion due to the long warm summer used.

The magnitude of the annual $\delta^{18}O$ and d changes due to this process are on the order of what we observe as annual changes in the snow profiles. The largest changes in the simulation occur during the warmest months and around the largest isotopic gradients. There was not a significant change in $\delta^{18}O$ observed beyond the uncertainty in

the snow profile averages, so we are not able to differentiate interannual $\Delta\delta^{18}O$ due to isotopic gradient diffusion from stratigraphic noise.

However, the interannual Δd in the summer layers was significant. Figure B1 shows a simulated interannual Δd due only to Johnsen et al. (2000) diffusion, using the 2019 mean snow profiles as a starting point. A large positive bias in d, up to 5 $^{o}/_{oo}$, can be seen in the summer layers after one year of isotopic-gradient-driven diffusion. This is similar to what we observe in the snow profiles (e.g. Figures 4(d) and 5(b)). However, the large positive excursion is preceded in time with a similarly large negative change in d. The Johnsen et al. (2000) model smooths isotopic signals, and shifts the d peaks downward, towards 'earlier' times. However, this behavior is not found in the observations.

Isotopic gradient diffusion is very likely at work in the near-surface snow during relatively warm months, particularly after the snow has been advected away from the influence of near-surface atmospheric winds (i.e. wind-pumping effects).

Open Research Section

All data used in this study are available for use and can be found at www.pangaea.de. Specific references follow. The bamboo snow stake data as described in Section 2.1 can be found at (Steen-Larsen, 2020a, 2020b; Harris Stuart et al., 2023). The snow surface isotope data as described in Section 2.2 can be found at (Hörhold et al., 2023; Hörhold, Behrens, Hoffmann, et al., 2022; Hörhold et al., 2022; Hörhold, Behrens, Wahl, et al., 2022). The raw measurements for the snow profile data as described in Section 2.3.1 can be found at (Behrens et al., 2023). The snow profile data with depth correction and age-depth model as described in Section 2.3.1, Section 2.4.1, and Section 2.4.2 be found at (Town et al., 2023).

Acknowledgments

This project has received funding from the European Research Council (ERC) under the European Union's Horizon 2020 research and innovation program: Starting Grant-SNOWISO (grant agreement 759526).

EastGRIP is directed and organized by the Centre for Ice and Climate at the Niels Bohr Instiute, University of Copenhagen. It is supported by funding agencies and institutions in Denmark (A. P. Møller Foundation, University of Copenhagen), USA (US Na-

tional Science Foundation, Office of Polar Programs), Germany (Alfred Wegener Institute, Helmholtz Centre for Polar and Marine Research), Japan (National Institute of Polar Research and Arctic Challenge for Sustainability), Norway (University of Bergen and Bergen Research Foundation), Switzerland (Swiss National Science Foundation), France (French Polar Institute Paul-Emile Victor, Institute for Geosciences and Environmental research), and China (Chinese Academy of Sciences and Beijing Normal University).

Many talented workers helped in the collection and measurement of the snow. Basile de Fleurian, Johannes Frietag, Abby Hughes, Emma Kahle, Martin Madsen, Hannah Meyer, Silje Smith-Johnsen, Alexandra Touzeau, Diana Vladimirova, and Tobias Zolles assisted in the field with snow collection and processing. Þorsteinn Jónsson and Rósa Ólafsdóttir assisted in the isotopic measurement of snow.

Author contributions are as follows: MST and HCSL designed the study. HCSL, AKF, SW, MB, MH, and AZ obtained the observational dataset. MB, MH, and AS analyzed the snow samples. MST and MB curated and processed the snow profile data set. MST performed the formal analysis and wrote the manuscript. HCSL, TJ, and SW contributed to the interpretation of the analyses. Reviews and edits were made by all coauthors. HCSL designed and acquired funding for this study and administrated the SNOW-ISO project.

References

Albert, M. R. (2002). Effects of snow and firm ventilation on sublimation rates. *Annals of Glaciology*, *35*, 52-56. doi: 10.3189/172756402781817194

Badgeley, J. A., Steig, E. J., & Dütsch, M. (2022, 12). Uncertainty in reconstructing paleo-elevation of the antarctic ice sheet from temperature-sensitive ice core records. *Geophysical Research Letters*, *49*. doi: 10.1029/2022GL100334

Behrens, M., Town, M. H. M. S., , & Steen-Larsen, H. C. (2023). *Snow profiles of stable water isotopes at the eastgrip deep drilling site, summer seasons 2016 - 2019* [data set]. PANGAEA. Retrieved from `PANGAEAdatasubmission: PDI-33944`

Blossey, P. N., Kuang, Z., & Romps, D. M. (2010). Isotopic composition of water in the tropical tropopause layer in cloud-resolving simulations of an idealized tropical circulation. *Journal of Geophysical Research Atmospheres*, *115*. doi:

963 10.1029/2010JD014554

964 Bolzan, J. F., & Pohjola, V. A. (2000, 9). Reconstruction of the undiffused seasonal
965 oxygen isotope signal in central greenland ice cores. *Journal of Geophysical Re-*
966 *search: Oceans*, *105*, 22095-22106. doi: 10.1029/2000jc000258

967 Buizert, C., Fudge, T. J., Roberts, W. H. G., Steig, E. J., Sherriff-Tadano, S., Ritz,
968 C., ... Schwander, J. (2021). *Antarctic surface temperature and elevation*
969 *during the last glacial maximum* (Vol. 372).

970 Casado, M., Landais, A., Picard, G., Arnaud, L., Dreossi, G., Stenni, B., & Prié,
971 F. (2021, 9). Water isotopic signature of surface snow metamorphism in
972 antarctica. *Geophysical Research Letters*, *48*. doi: 10.1029/2021GL093382

973 Casado, M., Landais, A., Picard, G., Münch, T., Laepple, T., Stenni, B., ... Jouzel,
974 J. (2018, 5). Archival processes of the water stable isotope signal in east
975 antarctic ice cores. *Cryosphere*, *12*, 1745-1766. doi: 10.5194/tc-12-1745-2018

976 Charles, C. D., Rind, D., Jouzel, J., Koster, R. D., & Fairbanks, R. G. (1994).
977 *Glacial-interglacial changes in moisture sources for greenland: Influences on*
978 *the ice core record of climate* (Vol. 263).

979 Ciais, P., & Jouzel, J. (1994). Deuterium and oxygen 18 in precipitation: Isotopic
980 model, including mixed cloud processes. *Journal of Geophysical Research*, *99*,
981 16793-16803. doi: 10.1029/94JD00412Ãŕ

982 Colbeck, S. C. (1983). Theory of metamorphism of dry snow. *Journal of Geophysical*
983 *Research*, *88*, 5475-5482. doi: 10.1029/JC088iC09p05475

984 Colbeck, S. C. (1989). Air movement in snow due to windpumping. *Journal of*
985 *Glaciology*, *35*, 209-213. doi: 10.3189/s0022143000004524

986 Colbeck, S. C. (1997). Model of wind pumping for layered snow. *Journal of Glaciol-*
987 *ogy*, *43*, 60-65. doi: 10.3189/s002214300000280x

988 Craig, H. (1961). Isotopic variations in meteoric waters. *Science*, *133*, 1702-1703.
989 doi: 10.1126/science.133.3465.1702

990 Craig, H., & Gordon, L. I. (1965). Deuterium and oxygen 18 variations m the ocean
991 and the marine atmosphere. In E. Tongiorgi (Ed.), *Stable isotopes in oceano-*
992 *graphic studies and paleotemperatures* (p. 9–130).

993 Cuffey, K. M., Clow, G. D., Alley, R. B., Stuiver, M., Waddington, E. D., & Saltus,
994 R. W. (1995). Large arctic temperature change at the wisconsin-holocene
995 glacial transition. *Science*, *270*, 455-458.

Cuffey, K. M., Clow, G. D., Steig, E. J., Buizert, C., Fudge, T. J., Koutnik, M., ... Severinghaus, J. P. (2016, 12). Deglacial temperature history of west antarctica. *Proceedings of the National Academy of Sciences of the United States of America*, *113*, 14249-14254. doi: 10.1073/pnas.1609132113

Dahl-Jensen, D., Albert, M. R., Aldahan, A., Azuma, N., Balslev-Clausen, D., Baumgartner, M., ... Zheng, J. (2013, 1). Eemian interglacial reconstructed from a greenland folded ice core. *Nature*, *493*, 489-494. doi: 10.1038/nature11789

Dansgaard, W. (1964, 11). Stable isotopes in precipitation. *Tellus*, *16*, 436-468. doi: 10.1111/j.2153-3490.1964.tb00181.x

Dee, S., Emile-Geay, J., Evans, M. N., Allam, A., Steig, E. J., & Thompson, D. M. (2015, 9). Prysm: An open-source framework for proxy system modeling, with applications to oxygen-isotope systems. *Journal of Advances in Modeling Earth Systems*, *7*, 1220-1247. doi: 10.1002/2015MS000447

Dütsch, M., Blossey, P. N., Steig, E. J., & Nusbaumer, J. M. (2019, 11). Nonequilibrium fractionation during ice cloud formation in icam5: Evaluating the common parameterization of supersaturation as a linear function of temperature. *Journal of Advances in Modeling Earth Systems*, *11*, 3777-3793. doi: 10.1029/2019MS001764

Ebner, P. P., Steen-Larsen, H. C., Stenni, B., Schneebeli, M., & Steinfeld, A. (2017, 7). Experimental observation of transient 18o interaction between snow and advective airflow under various temperature gradient conditions. *Cryosphere*, *11*, 1733-1743. doi: 10.5194/tc-11-1733-2017

Epstein, S., Sharp, R. P., & Gow, A. J. (1965). Six-year record of oxygen and hydrogen isotope variations in south pole firn. *JOURNAL OF GEOPHYSICAL RESEARCH*, *20*.

Fausto, R. S., As, D. V., Mankoff, K. D., Vandecrux, B., Citterio, M., Ahlstrøm, A. P., ... Box, J. E. (2021, 8). Programme for monitoring of the greenland ice sheet (promice) automatic weather station data. *Earth System Science Data*, *13*, 3819-3845. doi: 10.5194/essd-13-3819-2021

Filhol, S., & Sturm, M. (2015, 9). Snow bedforms: A review, new data, and a formation model. *Journal of Geophysical Research: Earth Surface*, *120*, 1645-1669. doi: 10.1002/2015JF003529

Fisher, D. A., Reeh, N., & Clausen, H. (1985). Stratigraphic noise in time series derived from ice cores. *Annals of Glaciology*, *7*, 76-83. doi: 10.3189/s0260305500005942

Fujita, K., & Abe, O. (2006, 9). Stable isotopes in daily precipitation at dome fuji, east antarctica. *Geophysical Research Letters*, *33*. doi: 10.1029/2006GL026936

Gkinis, V., Simonsen, S. B., Buchardt, S. L., White, J. W., & Vinther, B. M. (2014, 11). Water isotope diffusion rates from the northgrip ice core for the last 16,000 years - glaciological and paleoclimatic implications. *Earth and Planetary Science Letters*, *405*, 132-141. doi: 10.1016/j.epsl.2014.08.022

Gonfiantini, R. (1978). Standards for stable isotope measurements in natural compounds. *Nature*, *271*, 534-536. doi: http://dx.doi.org/10.1038/271534a0

Gow, A. J. (1965). On the accumulation and seasonal stratification of snow at the south pole. *Journal of Glaciology*, *5*, 467-477. doi: 10.3189/s002214300001844x

Grootes, P., Stuiver, M., White, J. W. C., Johnsen, S., & Jouzel, J. (1993). Comparison of oxygen isotope records from the gisp2 and grip greenland ice cores. *Nature*, *366*, 552–554.

Grootes, P. M., & Stuiver, M. (1987). *Ice sheet elevation changes from isotope profiles* (Vol. 170). IAHS Publ.

Guillevic, M., Bazin, L., Landais, A., Kindler, P., Orsi, A., Masson-Delmotte, V., ... Vinther, B. M. (2013). Spatial gradients of temperature, accumulation and 18o- ice in greenland over a series of dansgaard-oeschger events. *Climate of the Past*, *9*, 1029-1051. doi: 10.5194/cp-9-1029-2013

Harris Stuart, R., Faber, A.-K., Wahl, S., Hörhold, M., Kipfstuhl, S., Vasskog, K., ... Steen-Larsen, H. C. (2023). Exploring the role of snow metamorphism on the isotopic composition of the surface snow at eastgrip. *The Cryosphere*, *17*(3), 1185–1204. doi: 10.5194/tc-17-1185-2023

Hellmann, R., & Harvey, A. H. (2020, 9). First-principles diffusivity ratios for kinetic isotope fractionation of water in air. *Geophysical Research Letters*, *47*. doi: 10.1029/2020GL089999

Hörhold, M., Behrens, M., Hoffmann, A., Faber, A.-K., Kahle, E., Freitag, J., ... Steen-Larsen, H. C. (2022). *Snow stable water isotopes of a surface transect*

at the eastgrip deep drilling site, summer season 2017 [data set]. PANGAEA. Retrieved from PANGAEAdatasubmission:PDI-33947

Hörhold, M., Behrens, M., Vladimirova, D., Madsen, M., & Steen-Larsen, H. C. (2023). *Snow stable water isotopes of a surface transect at the eastgrip deep drilling site, summer season 2016* [data set]. PANGAEA. Retrieved from PANGAEAdatasubmission:PDI-33945

Hörhold, M., Behrens, M., Wahl, S., Faber, A.-K., Zuhr, A., Meyer, H., & Steen-Larsen, H. C. (2022). *Snow stable water isotopes of a surface transect at the EastGRIP deep drilling site, summer season 2019* [data set]. PANGAEA. Retrieved from https://doi.org/10.1594/PANGAEA.945563 doi: 10.1594/PANGAEA.945563

Hörhold, M., Behrens, M., Wahl, S., Faber, A.-K., Zuhr, A., Zolles, T., & Steen-Larsen, H. C. (2022). *Snow stable water isotopes of a surface transect at the EastGRIP deep drilling site, summer season 2018* [data set]. PANGAEA. Retrieved from https://doi.org/10.1594/PANGAEA.945544 doi: 10.1594/PANGAEA.945544

Hu, J., Yan, Y., Yeung, L. Y., & Dee, S. G. (2022, 6). Sublimation origin of negative deuterium excess observed in snow and ice samples from mcmurdo dry valleys and allan hills blue ice areas, east antarctica. *Journal of Geophysical Research: Atmospheres*, *127*. Retrieved from https://onlinelibrary.wiley.com/doi/10.1029/2021JD035950 doi: 10.1029/2021JD035950

Hudson, S. R., & Brandt, R. E. (2005). A look at the surface-based temperature inversion on the antarctic plateau. *Journal of Climate*.

Hughes, A. G., Wahl, S., Jones, T. R., Zuhr, A., Hörhold, M., White, J. W., & Steen-Larsen, H. C. (2021, 10). The role of sublimation as a driver of climate signals in the water isotope content of surface snow: Laboratory and field experimental results. *Cryosphere*, *15*, 4949-4974. doi: 10.5194/tc-15-4949-2021

Johnsen, S. (1977). Stable isotope homogenization of polar firn and ice. *In: Proc. Symp. on Isotopes and Impurities in Snow and Ice, I.U.G.G. XVI, General Assembly, 1975*, 210–219.

Johnsen, S., Clausen, H. B., Cuffey, K. M., Hoffrnann, G., Schwander, J., & Creyts, T. (2000). *Diffusion of stable isotopes in polar tirn and ice: the isotope effect in tirn diffusion.* Hokkaido University Press.

Johnsen, S., Dahl-Jensen, D., Gundestrup, N., Steffensen, J. P., Clausen, H. B., Miller, H., ... White, J. (2001). Oxygen isotope and palaeotemperature records from six greenland ice-core stations: Camp century, dye-3, grip, gisp2, renland and northgrip. *Journal of Quaternary Science*, *16*, 299-307. doi: 10.1002/jqs.622

Johnsen, S., & White, J. W. C. (1989). The origin of arctic precipitation under present and glacial conditions. *Tellus*, *418*, 452-468.

Jones, T. R., Cuffey, K. M., Roberts, W. H., Markle, B. R., Steig, E. J., Stevens, C. M., ... White, J. W. (2023, 1). Seasonal temperatures in west antarctica during the holocene. *Nature*, *613*, 292-297. doi: 10.1038/s41586-022-05411-8

Jones, T. R., Cuffey, K. M., White, J. W., Steig, E. J., Buizert, C., Markle, B. R., ... Sigl, M. (2017, 1). Water isotope diffusion in the wais divide ice core during the holocene and last glacial. *Journal of Geophysical Research: Earth Surface*, *122*, 290-309. doi: 10.1002/2016JF003938

Jones, T. R., Roberts, W. H., Steig, E. J., Cuffey, K. M., Markle, B. R., & White, J. W. (2018, 2). Southern hemisphere climate variability forced by northern hemisphere ice-sheet topography. *Nature*, *554*, 351-355. doi: 10.1038/nature24669

Jouzel, J., Alley, R. B., Cuffey, K. M., Dansgaard, W., Grootes, P., Hoffmann, G., ... White, J. (1997, 11). Validity of the temperature reconstruction from water isotopes in ice cores. *Journal of Geophysical Research: Oceans*, *102*, 26471-26487. doi: 10.1029/97JC01283

Jouzel, J., & Merlivat, L. (1984). *Deuterium and oxygen 18 in precipitation' modeling of the isotopic effects during snow formation* (Vol. 89).

Jouzel, J., Vimeux, F., Caillon, N., Delaygue, G., Hoffmann, G., Masson-Delmotte, V., & Parrenin, F. (2003, 6). Magnitude of isotope/temperature scaling for interpretation of central antarctic ice cores. *Journal of Geophysical Research Atmospheres*, *108*. doi: 10.1029/2002jd002677

Kahle, E. C., Steig, E. J., Jones, T. R., Fudge, T. J., Koutnik, M. R., Morris, V. A., ... White, J. W. (2021, 7). Reconstruction of temperature, accumulation rate, and layer thinning from an ice core at south pole, using a statistical inverse method. *Journal of Geophysical Research: Atmospheres*, *126*. doi: 10.1029/2020JD033300

Kavanaugh, J. L., & Cuffey, K. M. (2003). Space and time variation of 18o and d in antarctic precipitation revisited. *Global Biogeochemical Cycles*, *17*. doi: 10.1029/2002GB001910

King, J. C., & Turner, J. (2009). *Antarctic meteorology and climatology.* Cambridge University Press. doi: 10.1017/cbo9780511524967.006

Kochanski, K., Anderson, R. S., & Tucker, G. E. (2018, 7). Statistical classification of self-organized snow surfaces. *Geophysical Research Letters*, *45*, 6532-6541. doi: 10.1029/2018GL077616

Komuro, Y., Nakazawa, F., Hirabayashi, M., Goto-Azuma, K., Nagatsuka, N., Shigeyama, W., ... Dahl-Jensen, D. (2021, 3). Temporal and spatial variabilities in surface mass balance at the egrip site, greenland from 2009 to 2017. *Polar Science*, *27*. doi: 10.1016/j.polar.2020.100568

Kopec, B. G., Feng, X., Osterberg, E. C., & Posmentier, E. S. (2022, 10). Climatological significance of - line slopes from precipitation, snow pits, and ice cores at summit, greenland. *Journal of Geophysical Research: Atmospheres*. Retrieved from `https://onlinelibrary.wiley.com/doi/10.1029/2022JD037037` doi: 10.1029/2022JD037037

Laepple, T., Münch, T., Casado, M., Hoerhold, M., Landais, A., & Kipfstuhl, S. (2018, 1). On the similarity and apparent cycles of isotopic variations in east antarctic snow pits. *Cryosphere*, *12*, 169-187. doi: 10.5194/tc-12-169-2018

Lecavalier, B. S., Milne, G. A., Vinther, B. M., Fisher, D. A., Dyke, A. S., & Simpson, M. J. (2013, 3). Revised estimates of greenland ice sheet thinning histories based on ice-core records. *Quaternary Science Reviews*, *63*, 73-82. doi: 10.1016/j.quascirev.2012.11.030

Lorius, C., Jouzel, J., Raynaud, D., Hansen, J., & Treut, H. L. (1990). *The ice-core record: climate sensitivity and future greenhouse warming.*

Madsen, M. V., Steen-Larsen, H. C., Hörhold, M., Box, J., Berben, S. M., Capron, E., ... Dahl-Jensen, D. (2019, 3). Evidence of isotopic fractionation during vapor exchange between the atmosphere and the snow surface in greenland. *Journal of Geophysical Research: Atmospheres*, *124*, 2932-2945. doi: 10.1029/2018JD029619

Magnusson, B., Näykki, T., Hovind, H., Krysell, M., & Sahlin, E. (2017). *Handbook for calculation of measurement uncertainty in environmental laboratories* (Vol.

Nordtest Report TR 537 (ed. 4)).

Mahrt, L. (2014, 1). Stably stratified atmospheric boundary layers. *Annual Review of Fluid Mechanics*, *46*, 23-45. doi: 10.1146/annurev-fluid-010313-141354

Masson-Delmotte, V., Steen-Larsen, H. C., Ortega, P., Swingedouw, D., Popp, T., Vinther, B. M., ... White, J. W. (2015, 8). Recent changes in north-west greenland climate documented by neem shallow ice core data and simulations, and implications for past-temperature reconstructions. *Cryosphere*, *9*, 1481-1504. doi: 10.5194/tc-9-1481-2015

Mayewski, P. A., Meeker, L. D., Whitlow, S., Twickler, M. S., Morrison, M. C., Bloomfield, P., ... Wumkes, W. (1994). Changes in atmospheric circulation and ocean ice cover over the north atlantic during the last 41,000 years. *Science*, *263*, 1747-1751. doi: 10.1126/science.263.5154.1747

Merlivat, L., & Jouzel, J. (1979). Global climatic interpretation of the deuterium-oxygen 16 relationship for precipitation. *Journal of Geophysical Research*, *84*, 5029-5033. doi: 10.1029/JC084iC08p05029

Mojtabavi, S., Wilhelms, F., Cook, E., Davies, S. M., Sinnl, G., Jensen, M. S., ... Rasmussen, S. O. (2020, 11). A first chronology for the east greenland ice-core project (egrip) over the holocene and last glacial termination. *Climate of the Past*, *16*, 2359-2380. doi: 10.5194/cp-16-2359-2020

Münch, T., Kipfstuhl, S., Freitag, J., Meyer, H., & Laepple, T. (2016, 7). Regional climate signal vs. local noise: A two-dimensional view of water isotopes in antarctic firn at kohnen station, dronning maud land. *Climate of the Past*, *12*, 1565-1581. doi: 10.5194/cp-12-1565-2016

Münch, T., Kipfstuhl, S., Freitag, J., Meyer, H., & Laepple, T. (2017, 9). Constraints on post-depositional isotope modifications in east antarctic firn from analysing temporal changes of isotope profiles. *Cryosphere*, *11*, 2175-2188. doi: 10.5194/tc-11-2175-2017

Nakazawa, F., Nagatsuka, N., Hirabayashi, M., Goto-Azuma, K., Steffensen, J. P., & Dahl-Jensen, D. (2021, 3). Variation in recent annual snow deposition and seasonality of snow chemistry at the east greenland ice core project (egrip) camp, greenland. *Polar Science*, *27*. doi: 10.1016/j.polar.2020.100597

Neumann, T. A., & Waddington, E. D. (2004). Effects of firn ventilation on isotopic exchange. *Journal of Glaciology*, *50*, 183-192. doi: 10.3189/

1194 172756504781830150

1195 Neumann, T. A., Waddington, E. D., Steig, E. J., & Grootes, P. M. (2005). Non-
1196 climate influences on stable isotopes at taylor mouth, antarctica. *Journal of*
1197 *Glaciology*, *51*, 248-258. doi: 10.3189/172756505781829331

1198 Petit, J. R., Jouzel, J., Raynaud, D., Barkov, N. I., Barnola, J.-M., Basile, I., ...
1199 Stievenard, M. (1999). Climate and atmospheric history of the past 420,000
1200 years from the vostok ice core, antarctica the recent completion of drilling at
1201 vostok station in east. *Nature*, *399*, 429-436.

1202 Petit, J. R., White, J. W., Young, N. W., Jouzel, J., & Korotkevich, Y. S. (1991).
1203 Deuterium excess in recent antarctic snow. *Journal of Geophysical Research*,
1204 *96*, 5113-5122. doi: 10.1029/90JD02232

1205 Putnins, P. (1970). The Climate of Greenland. In O. S (Ed.), *World survey of clima-*
1206 *tology, vol 14* (p. 3-128). Barking, Essex, England: Elsevier Publishing Com-
1207 pany LTD.

1208 Ritter, F., Steen-Larsen, H. C., Werner, M., Masson-Delmotte, V., Orsi, A., Behrens,
1209 M., ... Kipfstuhl, S. (2016, 7). Isotopic exchange on the diurnal scale between
1210 near-surface snow and lower atmospheric water vapor at kohnen station, east
1211 antarctica. *Cryosphere*, *10*, 1647-1663. doi: 10.5194/tc-10-1647-2016

1212 Rohling, E. J., Sluijs, A., Dijkstra, H. A., Köhler, P., Wal, R. S. V. D., Heydt,
1213 A. S. V. D., ... Zeebe, R. E. (2012, 11). Making sense of palaeoclimate
1214 sensitivity. *Nature*, *491*, 683-691. doi: 10.1038/nature11574

1215 Schaller, C. F., Freitag, J., Kipfstuhl, S., Laepple, T., Steen-Larsen, H. C., & Eisen,
1216 O. (2016, 9). A representative density profile of the north greenland snowpack.
1217 *Cryosphere*, *10*, 1991-2002. doi: 10.5194/tc-10-1991-2016

1218 Shuman, C. A., Alley, R. B., Anandakrishnan, S., White, J. W. C., Grootes, P. M.,
1219 & Steams, C. R. (1995). Temperature and accumulation at the greenland
1220 summit: Comparison of high-resolution isotope profiles and satellite passive
1221 microwave brightness temperature trends. *JOURNAL OF GEOPHYSICAL*
1222 *RESEARCH*, *100*.

1223 Steen-Larsen, H. C. (2020a). *Snow surface accumulation measured using Bam-*
1224 *boo stake measurents, EastGRIP camp Greenland, May 2016* [data set]. PAN-
1225 GAEA. Retrieved from `https://doi.org/10.1594/PANGAEA.921855` doi: 10
1226 .1594/PANGAEA.921855

Steen-Larsen, H. C. (2020b). *Snow surface accumulation measured using SSA stake measurents, EastGRIP camp Greenland, May 2018* [data set]. PANGAEA. Retrieved from `https://doi.org/10.1594/PANGAEA.921853` doi: 10.1594/PANGAEA.921853

Steen-Larsen, H. C., Masson-Delmotte, V., Hirabayashi, M., Winkler, R., Satow, K., Prié, F., ... Sveinbjörnsdottír, A. E. (2014, 2). What controls the isotopic composition of greenland surface snow? *Climate of the Past*, *10*, 377-392. doi: 10.5194/cp-10-377-2014

Steen-Larsen, H. C., Masson-Delmotte, V., Sjolte, J., Johnsen, S. J., Vinther, B. M., Bréon, F. M., ... White, J. (2011). Understanding the climatic signal in the water stable isotope records from the neem shallow firn/ice cores in northwest greenland. *Journal of Geophysical Research Atmospheres*, *116*. doi: 10.1029/2010JD014311

Steffensen, J. P. (1985). Microparticles in snow from the south greenland ice sheet. *Tellus B*, *37 B*, 286-295. doi: 10.1111/j.1600-0889.1985.tb00076.x

Steffensen, J. P., Andersen, K. K., Bigler, M., Clausen, H. B., Dahl-Jensen, D., Fischer, H., ... White, J. W. (2008, 8). High-resolution greenland ice core data show abrupt climate change happens in few years. *Science*, *321*, 680-684. doi: 10.1126/science.1157707

Steig, E. J., Ding, Q., White, J. W., Küttel, M., Rupper, S. B., Neumann, T. A., ... Korotkikh, E. (2013, 5). Recent climate and ice-sheet changes in west antarctica compared with the past 2,000 years. *Nature Geoscience*, *6*, 372-375. doi: 10.1038/ngeo1778

Stevens, C. M., Verjans, V., Lundin, J. M., Kahle, E. C., Horlings, A. N., Horlings, B. I., & Waddington, E. D. (2020, 9). The community firn model (cfm) v1.0. *Geoscientific Model Development*, *13*, 4355-4377. doi: 10.5194/gmd-13-4355-2020

Touzeau, A., Landais, A., Morin, S., Arnaud, L., & Picard, G. (2018, 6). Numerical experiments on vapor diffusion in polar snow and firn and its impact on isotopes using the multi-layer energy balance model crocus in surfex v8.0. *Geoscientific Model Development*, *11*, 2393-2418. doi: 10.5194/gmd-11-2393-2018

Town, M. S., , & Steen-Larsen, H. C. (2023). *Water isotopologues of near-surface polar snow from short (1-m) snow cores, extracted from the eastgrip site on*

greenland ice sheet during summers 2017-2019. [data set]. PANGAEA. Retrieved from PANGAEAdatasubmission:PDI-33691

Town, M. S., Waddington, E. D., Walden, V. P., & Warren, S. G. (2008). Temperatures, heating rates and vapour pressures in near-surface snow at the south pole. *Journal of Glaciology*, *54*.

Town, M. S., Warren, S. G., Walden, V. P., & Waddington, E. D. (2008, 12). Effect of atmospheric water vapor on modification of stable isotopes in near-surface snow on ice sheets. *Journal of Geophysical Research Atmospheres*, *113*. doi: 10.1029/2008JD009852

Uemura, R., Masson-Delmotte, V., Jouzel, J., Landais, A., Motoyama, H., & Stenni, B. (2012). Ranges of moisture-source temperature estimated from antarctic ice cores stable isotope records over glacial-interglacial cycles. *Climate of the Past*, *8*, 1109-1125. doi: 10.5194/cp-8-1109-2012

Van Geldern, R., & Barth, J. A. (2012). Optimization of instrument setup and post-run corrections for oxygen and hydrogen stable isotope measurements of water by isotope ratio infrared spectroscopy (iris). *Limnology and Oceanography: Methods*, *10*, 1024-1036. doi: 10.4319/lom.2012.10.1024

Vinther, B. M., Jones, P. D., Briffa, K. R., Clausen, H. B., Andersen, K. K., Dahl-Jensen, D., & Johnsen, S. J. (2010, 2). Climatic signals in multiple highly resolved stable isotope records from greenland. *Quaternary Science Reviews*, *29*, 522-538. doi: 10.1016/j.quascirev.2009.11.002

Waddington, E. D., Steig, E. J., & Neumann, T. A. (2002). Using characteristic times to assess whether stable isotopes in polar snow can be reversibly deposited. *Annals of Glaciology*, *35*, 118-124. doi: 10.3189/172756402781817004

Wahl, S., Steen-Larsen, H. C., Reuder, J., & Hörhold, M. (2021, 7). Quantifying the stable water isotopologue exchange between the snow surface and lower atmosphere by direct flux measurements. *Journal of Geophysical Research: Atmospheres*, *126*. doi: 10.1029/2020JD034400

Wahl, S., Steen-Larsen, H. C., Hughes, A. G., Dietrich, L. J., Zuhr, A., Behrens, M., ... Hörhold, M. (2022, 10). Atmosphere-snow exchange explains surface snow isotope variability. *Geophysical Research Letters*, *49*. doi: 10.1029/2022gl099529

Werner, M., Jouzel, J., Masson-Delmotte, V., & Lohmann, G. (2018, 12). Rec-

onciling glacial antarctic water stable isotopes with ice sheet topography and the isotopic paleothermometer. *Nature Communications*, *9*. doi: 10.1038/s41467-018-05430-y

Werner, M., Langebroek, P. M., Carlsen, T., Herold, M., & Lohmann, G. (2011). Stable water isotopes in the echam5 general circulation model: Toward high-resolution isotope modeling on a global scale. *Journal of Geophysical Research Atmospheres*, *116*. doi: 10.1029/2011JD015681

Westhoff, J., Sinnl, G., Svensson, A., Freitag, J., Kjær, H. A., Vallelonga, P., ... Weikusat, I. (2022, 5). Melt in the greenland eastgrip ice core reveals holocene warm events. *Climate of the Past*, *18*, 1011-1034. doi: 10.5194/cp-18-1011-2022

Zuhr, A. M., Münch, T., Steen-Larsen, H. C., Hörhold, M., & Laepple, T. (2021, 10). Local-scale deposition of surface snow on the greenland ice sheet. *Cryosphere*, *15*, 4873-4900. doi: 10.5194/tc-15-4873-2021

Zuhr, A. M., Wahl, S., Steen-Larsen, H. C., Hörhold, M., Meyer, H., & Laepple, T. (2023). A snapshot on the buildup of the stable water isotopic signal in the upper snowpack at eastgrip on the greenland ice sheet.

Table 1: All data used in this study listed with units, a brief description, and data source. Uncertainties are 2σ standard deviation around the means.

Data	Units/Res.	Description	reference
Temperature	-28.5±14^oC	PROMICE weather station, hourly frequency, 2017-2019	Fausto et al. (2021)
Wind speed	5.26±4.6 m/s	data source and frequency same as above	same as above
Wind direction	W-SW	prevailing wind direction in all seasons, data source and frequency same as above	same as above
Annual accumulation (a)	134-157 mm/year	derived from from snow pits, 2009-2017	Komuro et al. (2021)
Annual accumulation (b)	145, 149 mm/year	snow pits, 2009-2016	Nakazawa et al. (2021)
Surface snow, 2016-2019	$\delta^{18}O$= ± 0.22$^o/_{oo}$; δD= ± 1.6 $^o/_{oo}$	Daily samples of 0-1 cm snow	Wahl et al. (2022), Section 2.2
Snow profiles, 2017	$\delta^{18}O$= ± 0.22$^o/_{oo}$; δD= ± 1.6 $^o/_{oo}$; 1-cm res, 0-10 cm; 2-cm res, 10-100 cm	Four (4) transects, 2 May 2017 - 11 August 2017, 40 profiles	Section 2.3
Snow profiles, 2018	same as above	Five (5) transects at six locations, 12 May 2018 - 06 August 2018, 35 profiles	Section 2.3
Snow profiles, 2019	same as above	Five (5) transects, 29 May 2019 - 24 July 2019, 25 profiles	Section 2.3

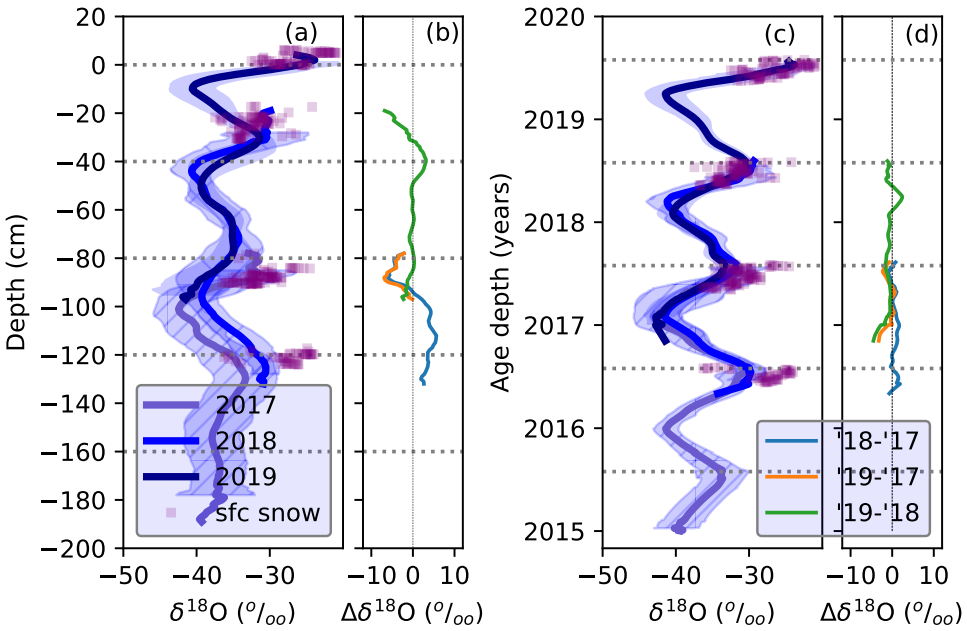

Figure 3: Mean $\delta^{18}O$ values from snow profiles and surface snow. The surface snow data (purple squares) are daily means from the 2016-2019 summer seasons. The snow profiles are mean values grouped by year of extraction (e.g. 2017, 2018, and 2019). Panel (a) shows the mean surface snow and snow profile $\delta^{18}O$ values as a function of relative depth. The surface is defined as 29 May 2019, the first day of snow profile sampling in 2019. Panel (b) shows the difference between each profile as a function of relative depth, representing the interannual change in $\delta^{18}O$. Panel (c) shows the mean surface snow and snow profile $\delta^{18}O$ values as a function of age-depth. Panel (d) shows the difference between each profile as a function of age-depth, representing the interannual change in $\delta^{18}O$. Shading represents 2σ standard error ($2\sigma_{\bar{x}}$). The horizontal lines in panels (a) and (b) are set at 40 cm, the approximate annual accumulation rate at EastGRIP. The horizontal lines in panels (c) and (d) represent 31 July of each year.

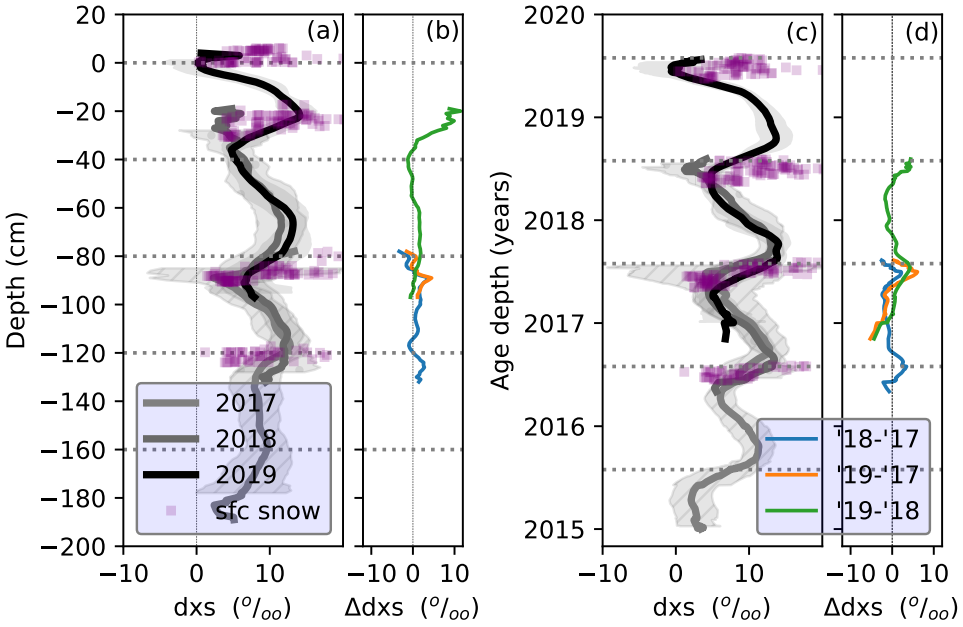

Figure 4: Mean d values from snow profiles and surface snow, as in Figure 3 for $\delta^{18}O$. The surface snow data (purple squares) are daily means from the 2016-2019 summer seasons. The snow profiles are mean values grouped by year of extraction (e.g. 2017, 2018, and 2019) with $2\sigma_{\bar{x}}$ as the shading. Panel (a) shows the mean surface snow and snow profile d values as a function of relative depth. The surface is defined as 29 May 2019, the first day of snow profile sampling in 2019. Panel (b) shows the difference between each profile as a function of relative depth. Panel (c) shows the mean surface snow and snow profile d values as a function of age-depth. Panel (c) shows the difference between each profile as a function of age-depth. Panels (b) and (d) represent the change in d between the different field seasons. Shading represents 2σ standard error ($2\sigma_{\bar{x}}$). The horizontal lines in panels (a) and (b) are set at 40 cm, the approximate annual accumulation rate at EastGRIP. The horizontal lines in panels (c) and (d) represent 31 July of each year.

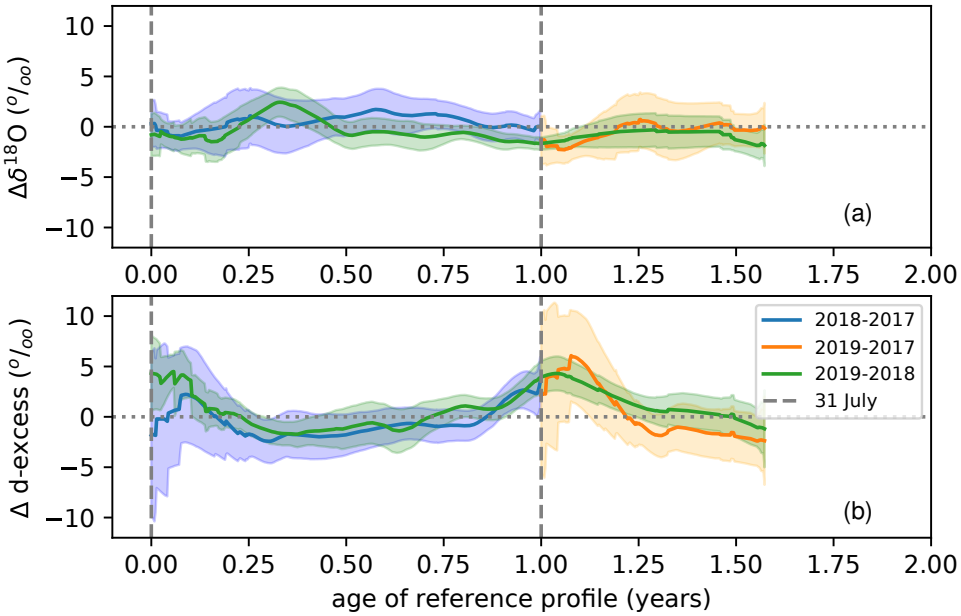

Figure 5: The change in $\delta^{18}O$ (panel (a)) and d (panel (b)) after one-to-two years of aging in the near surface snow. The change is determined as the difference between profiles shown in Figures 3(c) and 4(c), and plotted as a function of the age of the reference profile in the difference (e.g. 2018-2017 is plotted against the age of each snow layer from 2017). Seasons are marked on the horizontal axis, with snow depth increasing and time decreasing to the right.

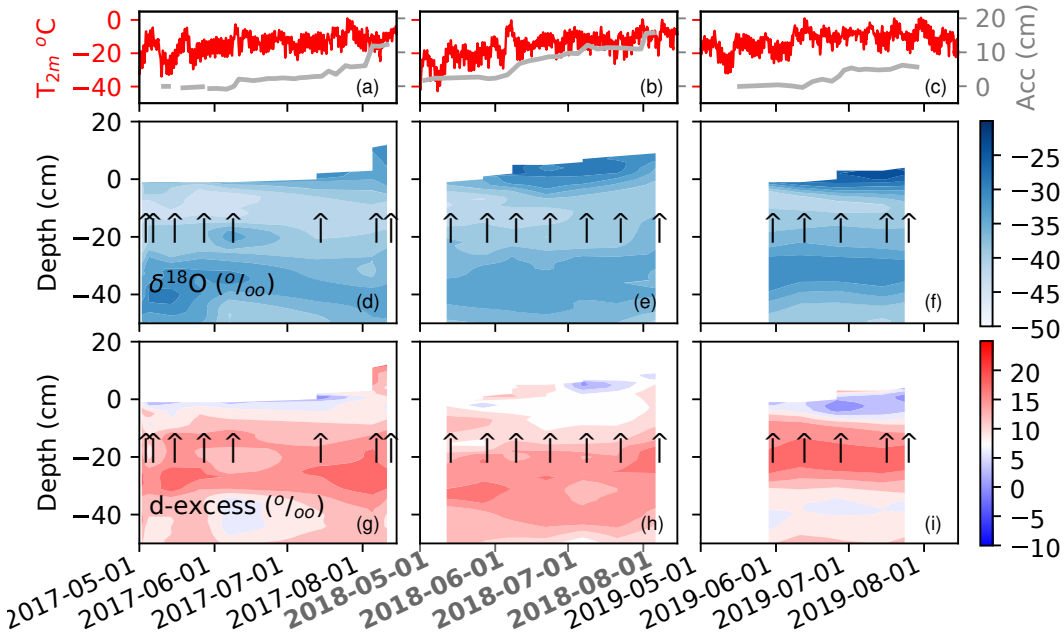

Figure 6: Mean $\delta^{18}O$ and d snow profiles plotted as depth (vertical axis) and date of extraction (horizontal axis) for the three summer field seasons 2017, 2018, and 2019. Panels (a-c) show the 2-m air temperature from the local PROMICE weather station and accumulation from the bamboo stake field. Panels (d-f) show the $\delta^{18}O$ content of the near-surface snow determined from mean $\delta^{18}O$ snow profiles. Each up arrow represents dates snow profiles were taken and averaged. For 2017, each arrow represents a mean of four snow profiles spaced approximately 50 m apart. For 2018 and 2019, each up arrow represents the mean of five snow profiles spaced approximately 50 m apart. Panels (g-i) are similar contour plots but for d. Note the vertical axis only extends to 50 cm depth because there is not subseasonal change below approximately 20-30 cm.

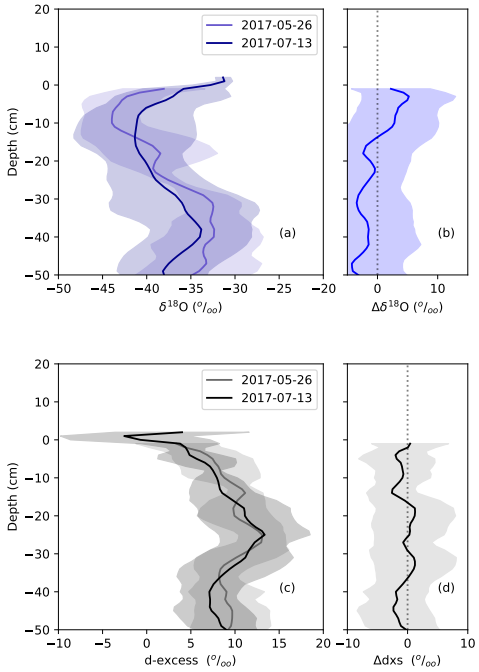

Figure 7: The mean isotopic change in near-surface from a low accumulation period during summer (25 May 2017 and 13 July 2017). Panels (a) and (c) are the mean snow profiles of $\delta^{18}O$ and d computed from four snow profiles each. Panels (b) and (d) show the isotopic change over this time period. Error bars are 2σ standard error.

Table A1: Table of annual statistics for $\delta^{18}O$ from the EastGRIP snow profiles shown in Figure 3. Columns are the year of extraction, e.g. *2019* represents July-July annual average from snow extracted during the 2019 summer field season (also the dark blue curve in Figure 3(c)). Rows are the age of the snow. The annual cycle is winter-centric, and computed from 31 July to 31 July. Units are in $^o/_{oo}$ and uncertainty is $2\sigma_{\bar{x}}$.

Extraction year	*2017*	*2018*	*2019*
Annual layer age			
07/2015 - 07/2016	-36.5±1.0	—	—
07/2016 - 07/2017	-37.2±1.1	-36.7±1.0	—
07/2017 - 07/2018	—	-35.7±1.0	-36.0±0.8
07/2018 - 07/2019	—	—	-34.9±1.4

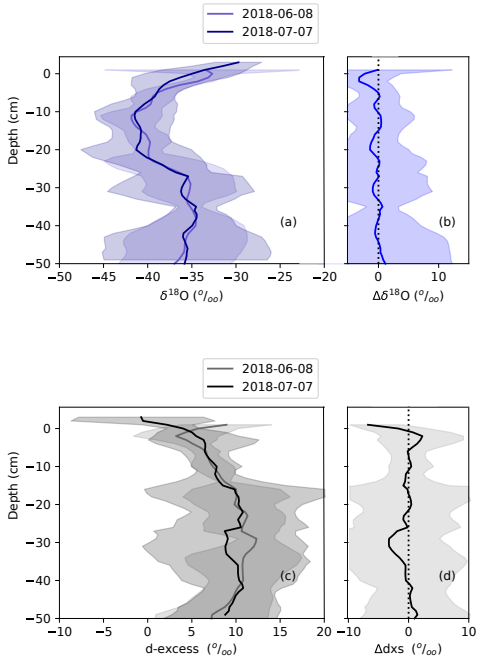

Figure 8: The mean isotopic change in near-surface from a low accumulation period during summer (08 June 2018 and 07 July 2018), similar to Figure 7. Panels (a) and (c) are the mean snow profiles of $\delta^{18}O$ and d computed from five snow profiles each. Panels (b) and (d) show the isotopic change over this time period. Error bars are 2σ standard error.

Table A2: Table of changes in $\delta^{18}O$ concentration after one or two years of aging in the EastGRIP firn from Figures 3(d) and 3(c), respectively. Columns are mean annual residuals, summer residuals (June/July), and non-summer residuals. Rows are the years between which the change is calculated. Units are in $^o/_{oo}$ and uncertainty is $2\sigma_{\bar{x}}$.

	Annual	*Summer*	*Non-summer*
$\overline{\delta^{18}O}_{y2}$- $\overline{\delta^{18}O}_{y1}$			
$\overline{\delta^{18}O}_{2018}$-$\overline{\delta^{18}O}_{2017}$	0.6±0.5	0.3±0.3	0.6±0.5
$\overline{\delta^{18}O}_{2019}$-$\overline{\delta^{18}O}_{2017}$	-0.9±0.6	-1.6±0.3	-0.7±0.5
$\overline{\delta^{18}O}_{2019}$-$\overline{\delta^{18}O}_{2018}$	-0.83±0.8	-1.1±0.4	-0.8±0.4

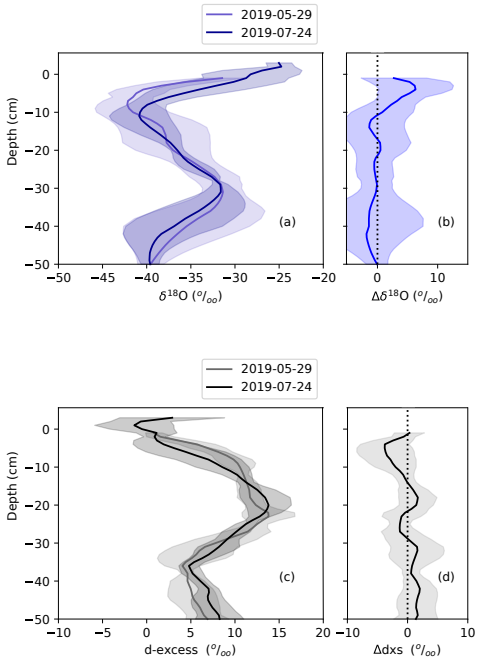

Figure 9: The mean isotopic change in near-surface from a low accumulation period during summer (29 May 2019 and 24 July 2019), similar to Figure 7. Panels (a) and (c) are the mean snow profiles of $\delta^{18}O$ and d computed from five snow profiles each. Panels (b) and (d) show the isotopic change over this time period. Error bars are 2σ standard error.

Table A3: Table of annual statistics for d from the EastGRIP snow profiles shown in Figure 3. Columns are the year of extraction, e.g. *2019* represents the black curve in Figure 4. Rows are the age of the snow. The annual cycle is winter-centric, and computed from 31 July to 31 July. Units are in $^o/_{oo}$ and uncertainty is $2\sigma_{\bar{x}}$.

Extraction year	*2017*	*2018*	*2019*
Annual layer age			
07/2015 - 07/2016	8.8±1.0	—	—
07/2016 - 07/2017	8.9±1.1	8.4±0.9	—
07/2017 - 07/2018	—	8.5±1.0	8.9±0.8
07/2018 - 07/2019	—	—	9.0±1.4

Table A4: Table of changes in d concentration after one or two years of aging the East-GRIP firn from Figures 4(a) and 4(c), respectively. Columns are mean annual residuals, summer residuals (June/July), and non-summer residuals. Rows are the years between which the change is calculated. Units are in $^{o}/_{oo}$ and uncertainty is $2\sigma_{\bar{x}}$.

	Annual	*Summer*	*Non-summer*
$\overline{d}_{\mathbf{y2}}$- $\overline{d}_{\mathbf{y1}}$			
$\overline{d}_{\mathbf{2018}} - \overline{d}_{\mathbf{2017}}$	-0.37±0.4	1.11±0.6	-0.89±0.4
$\overline{d}_{\mathbf{2019}} - \overline{d}_{\mathbf{2017}}$	-0.5±0.4	4.3±0.6	-1.8±0.4
$\overline{d}_{\mathbf{2019}} - \overline{d}_{\mathbf{2018}}$	0.4±0.4	3.3±0.6	-0.3±0.4

Table A5: Table of statistics for $\delta^{18}O$ and d from the EastGRIP surface snow, and d from near-surface summer snow less than one year old, as shown in Figure 3 and 4. Columns are the isotopologues. Rows are the sampling time period. Units are in $^{o}/_{oo}$ and uncertainty is $2\sigma_{\bar{x}}$.

	$\delta^{18}O_{sfc}$, summer	d_{sfc}, summer	d, summer snow profile, $<$ 1 year old
Field season			
06-08/2016	-27.7±1.2	8.55±1.5	
06-08/2017	-31.28±1.4	8.22±2.9	7.76±0.9
06-08/2018	-32.19±1.4	10.31±2.5	5.41±0.54
06-08/2019	-26.39±1.4	8.08±2.4	3.72±0.59

Table A6: Table of $\delta^{18}O$ vs δD composited by age and season. Summer is June-July. Winter is December-April. Units are in $(^{o}/_{oo})/(^{o}/_{oo})$ and uncertainty is 2σ.

	slope
All data	8.05±0.003
age < 1 year	7.91±0.004
Summer	*7.87±0.02*
Winter	*8.10±0.01*
1 year ≤ age < 2 years	8.18±0.006
Summer	*8.56±0.03*
Winter	*7.96±0.02*

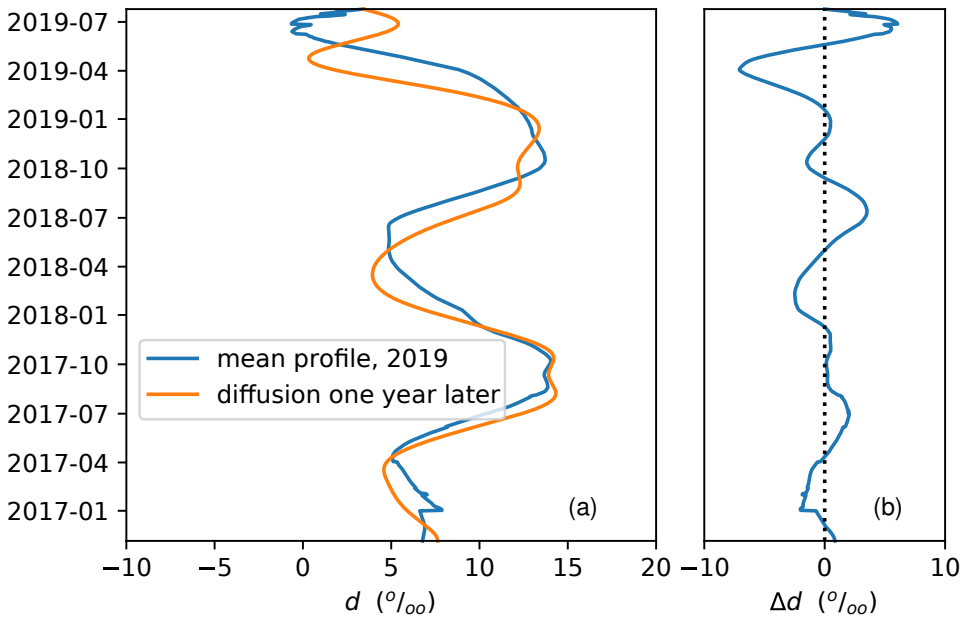

Figure B1: Panel (a) shows a simulation of the impact of isotopic-gradient-driven diffusion on the mean d snow profile from 2019 (blue curve) after one year of aging (orange curve). Panel (b) shows the change in d (Δd) after one year of aging. The simulation is described in detail in this Appendix B1.